POLITECNICO DI MILANO

Scuola di Ingegneria Industriale e dell'Informazione

Corso di Laurea in Ingegneria Matematica

AutoAssociative Kernel-Based and Bayesian Filter-Based Fault Detection in Industrial Components

Relatore: Dott. Piero BARALDI

Correlatore: Chiar.mo Prof. Enrico ZIO

Dott. Michele COMPARE

Tesi di Laurea di:

Pietro TURATI Matr. 784166

Anno Accademico 2012 – 2013

Index

List of Figures

List of Tables

Abstract

Fault Detection and Isolation (FDI) has drawn during the last decades the attention of industries due to its effectiveness in enhancing system performances and safety. According to prior information and monitoring systems available fault detection techniques are divided into two main categories: data-driven and model based methods.

In this thesis work, with respect to data-driven method, a modification of the traditional Auto Associative Kernel Regression method which enhances the signal reconstruction robustness is propounded. The modification is based on the definition of a new procedure for the computation of the similarity between the present measurements and the historical patterns used to perform the signal reconstructions. The underlying conjecture for this is that malfunctions causing variations of a small number of signals are more frequent than those causing variations of a large number of signals. An application to the condition monitoring of real industrial components is shown to improve the early detection of the occurrence of abnormal conditions and the correct identification of the signals triggering the detection.

With regard to model-based techniques, Particle Filtering (PF), a Bayesian filter-based method, is pursued due to its applicability to nonlinear model with non-additive non-Gaussian noise. In this thesis work, a PF approach, based on the

introduction of an augment discrete state pinpointing the particle evolution model, is propounded to tackle issues where Multiple Models (MM) are available for the description of the operation of an industrial component in normal and abnormal conditions. A smooth crack growth degradation problem has been considered to prove the effectiveness of the proposed method in the detection of the fault initiation and the identification of the degradation mechanism. The comparison of the obtained results with that of a literature method and an empirical statistical test has shown that the proposed method provides both an early detection of the fault initiation and an accurate identification of the degradation mechanism. A reduction of the computational cost is also achieved.

Sommario

Lo sviluppo negli ultimi decenni di strumentazioni relativamente economiche per il monitoraggio continuo ha stimolato l'interesse verso piani di manutenzione per impianti industriali di tipo dinamico. Essi, anziché ricorrere a manutenzioni programmate, mirano a valutare le condizioni di degrado dei componenti monitorati e sulla base di quest'ultime decidere se sia utile condurre delle manutenzioni. L'arresto non necessario di un impianto per sostituire dei componenti o per eseguire delle manutenzioni può, infatti, comportare alti costi economici. Nell'affrontare tale tematica sono divenuti essenziali:

- l'identificazione di condizioni di funzionamento anomalo;
- l'isolamento delle cause del malfunzionamento.

Il contributo che l'Identificazione e Isolamento di Anomalie (IIA) fornisce alle manutenzioni dinamiche è tale che nel corso degli ultimi decenni il mondo della ricerca e dell' industria ha rivolto un elevato interesse verso lo sviluppo di tecniche sempre più efficaci. Una buona IIA è caratterizzata da una rapida individuazione delle anomalie e da un'accurata identificazione del processo e delle cause di degrado ad esse associate. Le tecniche di IIA si possono classificare in due categorie principali:

- metodi basati su *modelli espliciti* del comportamento del componente.
- metodi basati sulle *osservazioni storiche* (OS) del comportamento del componente.

In questo lavoro di tesi sono stati sviluppati contributi innovativi in entrambe le categorie. Generalmente i metodi basati sulle osservazioni storiche identificano eventuali anomalie nel comportamento del componente ricorrendo a modelli empirici costruiti con dati storici disponibili.

Infatti data un'osservazione i modelli empirici permettono di indentificare un eventuale guasto. Tale processo si basa sul confronto tra l'osservazione e il valore ricostruito dal modello, il quale corrispondente al corretto funzionamento del componente. La modalità con cui viene effettuata la ricostruzione è ciò che contraddistingue i diversi metodi. Questo lavoro di tesi si è focalizzato sull'AutoAssociative Kernel Regression (AAKR) che propone una ricostruzione come media pesata delle osservazioni già raccolte durante condizioni di normale funzionamento. I pesi possono essere considerati come un indice di similarità tra il comportamento osservato e l'osservazione storica. In questo studio viene proposta una modifica all'algoritmo utilizzato per il calcolo dei pesi al fin di ottenere delle ricostruzioni più robuste. La modifica apportata si basa sull'introduzione di una proiezione delle osservazioni in un nuovo spazio degli stati in modo da considerare la maggior frequenza di accadimento di guasti che coinvolgono un numero ridotto di segnali rispetto a guasti che coinvolgono un numero maggiore di essi. Il procedimento è stato testato durante il monitoraggio delle condizioni di alcuni componenti di un impianto di produzione di energia elettrica. I risultati mostrano come il metodo introdotto sia in grado di identificare prima del AAKR tradizionale l'occorrenza di anomalie nei componenti. Inoltre esso è in grado di isolare i sensori che realmente monitorano l'anomalia del componente, consentendo di eseguire delle manutenzioni mirate. Infine i costi computazionali sono paragonabili a quelli del metodo tradizionale, questo permette la sua applicazione a sistemi di monitoraggio continui..

Per quanto riguarda i metodi basati su modelli espliciti questo lavoro è focalizzato sul *Particle Filtering* (PF) poiché consente di trattare modelli espliciti con un numero di restrizioni molto ridotto rispetto alle altre tecniche già proposte in letteratura, come il filtro di Kalman e le sue generalizzazioni. In particolare il PF è in grado di trattare modelli non lineari soggetti a rumori non additivi e non Gaussiani attraverso l'utilizzo di una distribuzione empirica. In molti casi il funzionamento o lo stato di degrado di un componente può essere

descritto da Modelli Multipli (MM). Generalmente un modello di riferimento è disponibile per descrivere le condizioni di normalità e diversi modelli per descrivere i possibili stati di guasto o di degrado. La fase di isolamento in questo ambito consiste nell'identificare quale sia il modello che maggiormente spiega le osservazioni raccolte. In letteratura questo problema è già stato affrontato utilizzando un diverso PF per ogni modello disponibile e andando a identificare a posteriori quale delle filtrazioni ottenute, quindi l'associato modello, sia la più adatta ai dati raccolti. D'altro canto tale strategia richiede un grosso sforzo computazionale dovuto all'elevato numero di particelle da simulare. Per evitare di simulare diversi gruppi di particelle è stato proposto di introdurre una variabile discreta indicante esplicitamente il modello secondo il quale esse evolvono. In questo modo è sufficiente utilizzare un unico PF riducendo quindi il costo computazionale. Inoltre il PF così ottenuto, durante la fase di aggiornamento della distribuzione empirica, è in grado di promuovere le particelle che evolvono secondo il modello più consono all'osservazione raccolta, rendendolo auto adattativo. Questo consente di isolare il modello più verosimile alle osservazioni mediante la marginalizzazione della distribuzione empirica sulla variabile discreta associata ai modelli. La validità di tale metodo è stata testata su un problema di degrado di un componente sotto sforzo. In particolare si è considerata la propagazione di una crepa al suo interno, descritta attraverso tre modelli di degrado non necessariamente lineari e altamente stocastici. Questo è il primo lavoro, per quanto ne sia a conoscenza l'autore, che tale tipo di approccio venga applicato ad un problema di diagnostica. I risultati ottenuti mostrano come tale metodo sia risultato efficace nel rapido riconoscimento del degrado del componente ed in particolare nel diagnosticare la fase di degrado associata.

1

Introduction

In recent years, the development of relatively affordable on-line monitoring technology has yielded a growing interest in dynamic maintenance paradigms such as Condition-Based Maintenance (CBM). This is based on tracking the health conditions of the monitored industrial component and, on this basis, making maintenance decisions. To do this, two fundamental issues are addressed:

- detection, i.e., the recognition of a deviation from the normal operating conditions;
- isolation or diagnostics, i.e., the characterization of the abnormal state of the component.

In principle, an effective fault detection system is characterize by a prompt detection of the deviation of the component from the normal conditions of functioning: the earlier the detection time, the larger the time available to plan optimal maintenances intervention. This is particularly important for safety critical components whose failure and malfunctioning can lead to undesired

consequences to the environment and the humans. Thus, the adoption of a condition based maintenance policy is expected to increase the availability of the industrial component thank to the possibility of avoiding unnecessary downtime due to unnecessary maintenance interventions or to the possibility of preventing from the corrective maintenance due to unexpected failure. Furthermore the overall safety of the industrial plant is expected to be enhanced thanks to the capability of promptly detecting anomalous behavior of the industrial component and thus to avoid failures.

The appealing potential of the CBM approach in improving the maintenance performance has boosted research and industry efforts in tackling FDI issues, as witnessed by the considerable amount of related literature (see ([7], [29], [43], [44], [45], [51] for surveys). FDI techniques can be divided into two main categories: data-driven methods, which resort to field data to build empirical models of the equipment behavior and model-based approaches, which utilize mathematical models to describe the behavior of the component. In both cases, the detection of a change in the component state is typically based on the comparison of the output of the model with the measurement acquired from the operating component.

Data-driven (empirical) models are employed in those cases in which analytical models of the component behavior are not available and cannot be easily developed. A data-driven condition monitoring approach typically exploits an empirical model which reconstructs the values of the signals expected in normal conditions of the components. During operation, observed signal measurements

are compared with the reconstructions provided by the model: abnormal components conditions are detected when the reconstructions are remarkably different from the measurements. Several empirical reconstruction modeling technique have been applied for condition monitoring of industrial components such as AutoAssociative Kernel Regression (AAKR [3]), Principal Component Analysis (PCA [19],[24]), Evolving Clustering Method (ECM), Support Vector Machine (SVM, [28]) , AutoAssociative (AA) and Recurrent (R) Neural Networks (NN) ([8],[23],[38],[48]), Local Gaussian Regression (LGR, [35][41]). In this work, we consider AAKR which has been shown to provide more satisfactory performance in many cases, has often proven superior to other methods like, e.g., ECM and PCA [15] and is less computationally demanding than methods, e.g., AANN and RNN. Notice that small computational cost is an important desideratum for condition monitoring systems, since they are typically used online, during component operation and, thus the outcome of the FDI should be provided to the maintenance decision makers as soon as possible. Applications of the AAKR method to fault detection in industrial components have been proposed in [3], [4], [5], [15], [16], [20], [26] and [27]. They have shown the low robustness of the method in case of abnormal conditions, especially when the observed signals are highly correlated. By robustness, here we intend the property such that, in case abnormal or noisy measurements are collected, the reconstruction of the signal expected in normal condition provided by the empirical model, is not affected by errors or drift. Low robustness entails a delay in the detection time and an incorrect identification of the signal impacted by

abnormal conditions (Fault Isolation). In the first part of the thesis work, a novel modified AAKR method is presented to overtake these limitations of the traditional AAKR method. The modification of the AAKR method is based on the definition of a new procedure for the computation of the similarity between the present measurements and the historical patterns used to perform the signal reconstructions. The rationale behind this proposition of the modification is the attempt to privilege those abnormal conditions caused by the most frequently expected malfunctions and failures. The performance of the proposed method will be tested on real data collected from an industrial plant for energy production.

In the second part of this thesis work, model-based methods which exploit mathematical models to describe the component behavior in normal and abnormal conditions, are considered. They usually estimate physical quantities which are related to the component health state or degradation level. For example, monitoring of structures can be based on the estimate of the length of cracks. In particular, a number of filtering algorithms have been successfully applied to FDI, which use discretized differential equations to describe the degradation evolution, and stochastic noises to take into account the associated aleatory uncertainty. For example, Kalman Filter (KF) has been adopted to detect incidents on freeways [47], and to set a CBM policy on turbine blades affected by creep [6]. However, KF suffers from a limited applicability, due to the stringent hypotheses of model linearity and Gaussian noise, which are required and are often not compatible with practical FDI issues. Thus, some generalizations of KF

such as Extended Kalman Filter (EKF [36], [37]) and Unscented Kalman Filter (UFK, [30]) have been proposed to relax the strictness of the KF's hypotheses. Nonetheless, there are still situations where these filtering approaches fail, due to high non linearity or the presence of non-Gaussian noise.

In this framework, Particle Filtering (PF) has drawn the attention of the researchers due to its wide range of applicability to nonlinear, non-Gaussian models ([2],[17],[46],[49] and [50]). In particular, PF has been adopted as a FDI tool within the Multi-Model (MM) systems framework, where the description of the possible component abnormal evolutions relies on a set of models [31]. In this setting, detection aims at identifying when the component starts to leave the nominal model, representing its behavior in normal condition, whereas diagnostics consists in selecting the model that best fits the current behavior of the component. The approaches in [1], [12] and [33] are based on the simulation of parallel swarms of particles according to each operating model and on the selection, via likelihood analysis between the simulated trajectories and the gathered measurements, of the model that best fits the observations. However, this entails an increasing computational cost due to the large number of particles that must be simulated. A promising approach introduced in ([39], [42]) propound to augment the state vector of the particle with a Boolean variable concerning the state of health of the component. This allows to take into account the evolution of the component state avoiding to increase the number of particles to be simulated. In this thesis work, this idea is applied for the first time, at the best of the author's knowledge, to a nonlinear, highly non-Gaussian

smoothly degradation process of an industrial component subject to an high measurement error. The case study concerns a component subjected to fatigue crack growth, whose degradation process can be described by three different models. The performances obtained by the proposed approach will be compared with those obtained from a multiple swarms method [12] and from a statistical sequential test. Furthermore another novel contribution of this thesis work is to apply this approach for diagnostic, since it has never been exploited for monitoring components where different type of abnormal behavior can occur. The objective of the novel method is to provide, at a reduced computational cost, an early detection of the fault initiation and a prompt identification of the degradation phase. The remainder of the thesis work is organized as follow: in Chapter 2, the data-driven FDI is tackled according to the AAKR method. A novel modified AAKR method is here proposed and applied to a real case study; in Chapter 3 the Bayesian Filter-Based FDI is proposed. Application to a crack degradation process and comparison of the results with those obtained from an MS method is also reported. Finally, Chapter 4 presents the conclusions and describes the potential future direction of research. In appendix an introduction to the PF algorithm is presented.

2

AutoAssociative Kernel-Based

Data-driven (empirical) models are employed in those cases in which analytical models of the component behavior are not available and cannot be easily developed. Data-driven models are built using historical data collected during operation and require a limited number of hypotheses ([27],[44],[45]). A data-driven condition monitoring approach is typically based on an empirical model which reconstructs the values of the monitored signals expected in normal conditions of the components. During operation, signal measurements are compared with the reconstructions provided by the empirical model: abnormal conditions are detected when the reconstructions are remarkably different from the measurements.

Several empirical reconstruction modeling technique have been applied for condition monitoring of industrial components ([3],[4],[5],[15],[19],[23] and [24]). These methods can provide accurate reconstructions of the measured signals under normal operations, but they often tend to be not robust. By robustness, here it is intended the property such that, in case abnormal or noisy measurements are collected, the reconstruction of the signal expected in normal condition provided by the empirical model, is not affected by error or drift. In [3], it has been shown that in case of abnormal conditions, empirical models may

provide reconstructions of the measured signals which are not estimating the expected values of the signals in normal conditions, especially when the measured signals are highly correlated. In particular, it has been shown that the reconstruction provided by AAKR of an anomalous transient characterized by a drift of one signal can be not satisfactory for two reasons: 1) the reconstruction of the signal affected by the drift tends to assume values in the middle between the drifted and the expected values of the signal in normal conditions 2) the reconstructions of other signals not affected by the drift tend, erroneously, to be different from the signal measurements, (this latter effect is usually referred to with the term 'spill-over'). The consequence of 1) is a delay in the detection of abnormal conditions, whereas the consequence of 2) is that the condition monitoring system, although it correctly triggers an abnormal condition alarm, it is not able to correctly identify the signal that triggers the alarm.

These limitations of reconstruction models have been already studied in ([3],[15] and [20]). Solution to these problems have been proposed, which amount to try to exclude the signals with abnormal behaviors from the set of input signals used to perform the reconstruction

In ([3], [4] and [16]),the authors have propounded ensembles of reconstruction models handling different sets of input signals. In case of an anomaly impacting the behavior of a generic signal, only the few models fed by that signal provide non robust reconstructions, whereas all the other models provide correct reconstructions. Another solution has been embraced in [20] whereby a ponderation matrix iteratively modifies its elements to reduce the contribution of abnormal signals to the reconstruction but the convergence of the method to correct signal reconstructions has not been yet demonstrated. All these solution come at high computational costs.

The objective of this chapter is to propose a robust signal reconstruction method with low computational cost and i) capable of early detection of abnormal conditions, ii) accurate in the reconstructions of the values of the signals impacted by the abnormal conditions and iii) resistant to the spill-over effect.

The proposed method is based on the modification of the measure of similarity used by the Auto-Associative Kernel Regression (AAKR) method. Whereas the traditional AAKR employs measures of similarity based on Euclidean or Mahalanobis distances, the proposed method introduces a penalty vector which reduces the contribution provided by those signals which are expected to be impacted by the abnormal conditions. The rationale behind this proposition of the modification is the attempt to privilege those abnormal conditions caused by the most frequently expected malfunctions and failures. The performance of the proposed method has been tested on real data collected from an industrial plant for energy production. The remainder of the chapter is organized as follows.

In Section 2.1, the fault detection problem is introduced. In Section 2.2 the AAKR method is briefly recalled. Section 2.3 shows the limitation of the traditional AAKR approach to condition monitoring and states the objectives of the present chapter. In Section 2.4, the proposed modification of the traditional AAKR is described and discussed. In Section 2.5, the application of the proposed method to a real case study concerning the monitoring of 6 signals in an industrial plant for energy production is discussed. Finally, in Section 2.6 some conclusions are drawn.

2.1 Fault Detection with Empirical Model

In this chapter condition monitoring scheme for fault detection as shown in Fig. 2.1 is considered.

The (empirical) model reproducing the plant behavior in normal conditions receives in input the vector, $\vec{x}^{obs}(t)$, containing the actual observations of the *J* signals monitored at the present time, t, and produces in output the reconstructions, $\hat{\vec{x}}_{nc}(t)$, i.e. the values that the signals are expected to have in normal conditions. If the actual conditions at the time t are, instead, the residuals, $\Delta\vec{x} = \vec{x}^{obs}(t) - \hat{\vec{x}}_{nc}(t)$ i.e. the variations between the observation and the reconstructions, are larger and can be detected by exceedance of a prefixed thresholds by at least one signal.

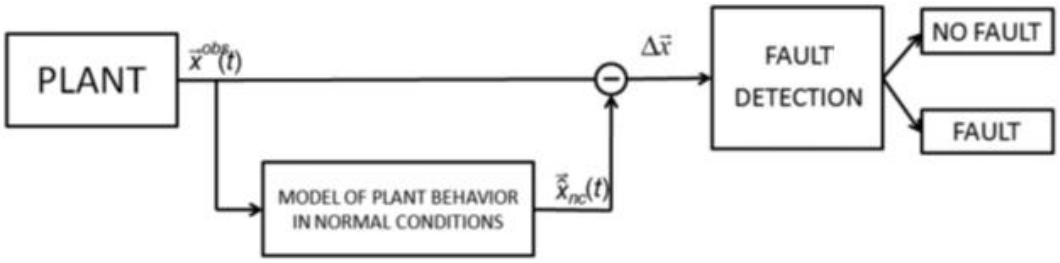

Fig. 2.1 Scheme of condition monitoring for fault detection

2.2 AutoAssociative Kernel Regression (AAKR)

The basic idea behind AAKR is to reconstruct at time t the values of the signals expected in normal conditions, $\hat{\vec{x}}_{nc}(t)$, on the basis of a comparison of the currently observed signals measurements (also referred to as test pattern), $\vec{x}^{obs}(t) = [x^{obs}(t,1), \dots, x^{obs}(t,J)]$, and of a set of historical signals measurements collected during normal condition of operation. In practice, AAKR performs a mapping from the space of the measurements of the signals $\vec{x}^{obs}(t)$ to the space of the values of the signals expected in normal conditions, $\hat{\vec{x}}_{nc}(t)$:

$$\hat{\vec{x}}_{nc}(t) = \varphi\left(\vec{x}^{obs}(t)|X^{obs-nc}\right) : \mathbb{R}^J \rightarrow \mathbb{R}^J \qquad (2.1)$$

where $\bar{\bar{X}}^{obs-nc}$ indicates a $N \times J$ matrix containing *N* historical observations of the J signals performed in normal-conditions. Since the mapping is independent from the present time, t, at which the signals observations are performed, the present time t will be omitted from the notations. Thus, $x^{obs}(j)$, j=1, …, J, indicates the value of signal j at the present time. The reconstruction of the expected values of the signals in normal conditions, $\hat{\vec{x}}_{nc} = [\hat{x}_{nc}(1), \dots, \hat{x}_{nc}(J)]$, is performed as a weighted sum of the available historical observations; for the generic j-th element of $\hat{\vec{x}}_{nc}$, this is:

$$\hat{x}_{nc}(j) = \frac{\sum_{k=1}^{N} w(k) \cdot x^{obs-nc}(k,\ j)}{\sum_{k=1}^{N} w(k)} \tag{2.2}$$

The weights, $w(k)$, measure the similarity between the test pattern, $\vec{x}^{obs}$, and the k-th historical observation vector, $\vec{x}^{obs-nc}(k)$. They are evaluated through a kernel, Ker, i. e., a scalar function which can be written as a dot product. From the mathematical point of view, a Kernel is a function:

$$Ker: \mathbb{R}^J \times \mathbb{R}^J \rightarrow \mathbb{R}\ s.t.\ \exists \boldsymbol{\phi}: \mathbb{R}^J \rightarrow \mathcal{H}, Ker(\vec{x}, \vec{y}) = \langle \boldsymbol{\phi}(\vec{x}), \boldsymbol{\phi}(\vec{y}) \rangle \tag{2.3}$$

where $\boldsymbol{\phi}$ is a map from the observation space $\mathbb{R}^J$ in a (possibly countable infinite dimensional) Euclidean space $\mathcal{H}$ and $\langle .,. \rangle$ denots the dot product. Traditional AAKR adopts as Ker function the Gaussian Radial Basis Function (RBF) with bandwidth parameter h, i.e.:

$$w(k) = Ker\left(\vec{x}^{obs}, \vec{x}^{obs-nc}(k)\right) = \frac{1}{\sqrt{2\pi h^2}} e^{-\frac{\left\|\vec{x}^{obs} - \vec{x}^{obs-nc}(k)\right\|^2}{2h^2}} \tag{2.4}$$

Notice that, according to Mercer's theorem [10], eq. (2.4) can be seen as a dot product in a countable infinite dimensional Euclidean space:

$$e^{-\frac{1}{2}\left\|\vec{x}^{obs} - \vec{x}^{obs-nc}(k)\right\|_2^2} == \sum_{i=0}^{\infty} \frac{\left(\vec{x}^{obs^T} \vec{x}^{obs-nc}(k)\right)^i}{i!} e^{-\frac{1}{2}\|\vec{x}^{obs}\|_2^2} e^{-\frac{1}{2}\left\|\vec{x}^{obs-nc}(k)\right\|_2^2} \tag{2.5}$$

In fault detection applications, Euclidean and Mahalanobis distances are typically used to compute the distance in the Gaussian RBF. In this work, in order to

account for differences in the scale and variability of the different signals, a Mahalanobis distance is used, defined by the covariance matrix, *S*, such that:

$$\left\|\vec{x}^{obs} - \vec{x}^{obs-nc}(k)\right\|_{mahal}^{2} = \left(\vec{x}^{obs} - \vec{x}^{obs-nc}(k)\right)^{T} S^{-1} \left(\vec{x}^{obs} - \vec{x}^{obs-nc}(k)\right) \tag{2.6}$$

Assuming independence between the signals, S is given by:

$$S = \begin{bmatrix} \sigma_1^2 & \dots & 0 \\ \vdots & \ddots & \vdots \\ 0 & \dots & \sigma_j^2 \end{bmatrix} \tag{2.7}$$

where σ_j^2 indicates the estimated variance of signal j in the historical observations. Alternatively, instead of using (2.6) and (2.7), one can obtain the same results by mapping the data in a normalized space according to:

$$y(j) = \frac{x(j) - \mu_j}{\sigma_j} \tag{2.8}$$

where μ_j is the mean value of signal j in the historical dataset, and by applying a Gaussian kernel with Euclidean distance in the normalized space.

2.3 Limitations in the Use of AAKR for Signal Reconstruction

The availability of relatively affordable monitoring technology typically leads to the installation of a great number of sensors, which are often monitoring signals characterized by high degrees of correlation. In this context of correlated signals, AAKR reconstructions performed in abnormal conditions have been shown to be not satisfactory from the point of view of the robustness: the obtained reconstructions are not accurately estimating the values of the signals expected in normal conditions [4]. This effect is well illustrated by the following case study concerning the monitoring of a component of a plant for the production of energy. A dataset containing the real evolution of 6 highly correlated signals (Table 2.1) for a period of 1 year with sampling frequency of 5200

measurements/year has been used to develop an AAKR reconstruction model. Then, in order to artificially simulate an abnormal condition, a linearly increasing drift has been added to the real values of one of the six signals for a period of 600 time steps: these drifted data have not been used to develop the AAKR model. Fig. 2.2 (top) shows the drifted signal, whereas Fig. 2.2 bottom shows the residuals of the reconstruction of the drifted signal (left) and of another signal not affected by the abnormal condition (right). Notice that the obtained reconstructions are not robust: 1) the residuals of the drifted signal are not following the applied drift 2) the residuals of the other signal is erroneously deviating from 0.

	S1	**S2**	**S3**	**S4**	**S5**	**S6**
S1	1	0.97	0.98	0.98	0.99	0.98
S2	0.97	1	0.95	0.99	0.98	0.96
S3	0.98	0.95	1	0.96	0.99	0.99
S4	0.98	0.99	0.96	1	0.98	0.97
S5	0.99	0.98	0.99	0.98	1	0.99
S6	0.98	0.96	0.99	0.97	0.99	1

Table 2.1 degree of correlation between the signals

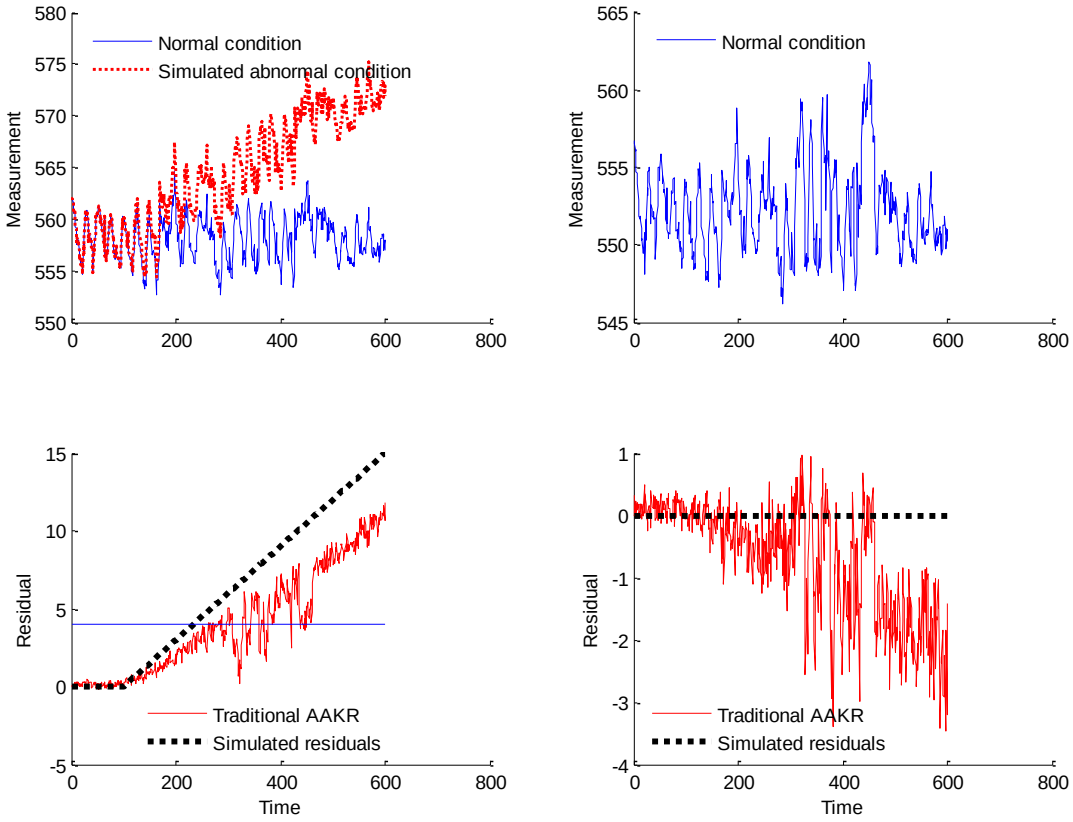

Fig. 2.2 Top (left): the continuous line represents signal 1 values in normal conditions, the dotted line the signal values in the simulated abnormal conditions; top (right): evolution of signal 3 (not affected by the abnormal conditions). Bottom: the continuous line represents the residuals obtained by applying the traditional AAKR reconstruction, the dotted line the residual which would be obtained by a model able to perfectly reconstruct the signal behavior in normal conditions.

From the practical point of view of the fault detection, two problems arise in relation to the low robustness of the reconstruction:

1) delay in the detection of the abnormal condition (an alarm is usually triggered when the residuals exceed prefixed thresholds).
2) detection of abnormal conditions on signals different from those which are actually impacted by the abnormal behavior (spill-over).

With regards to the latter, the identification of the signals which are affected by the abnormal conditions is critical since it can allow to identify the cause of abnormality and, thus, to properly plan the maintenance intervention.

2.4 Modified AAKR

In order to enhance the AAKR robustness, it is propose to modify the computation of the weights as the traditional AAKR (eq. (2.4)). The basic ideas underling the proposed modification are (a) to identify the signals affected by abnormal behaviors and (b) to reduce their importance in the computation of the similarity between the test pattern and the historical observations.

With respect to (a), it is assumed that the probability of occurrence of a fault causing variations on a large number of signals is lower than that of a fault causing variations on a small number of signals:

$$P(S_{faul\,1}) < P(S_{faul\,2}) \text{ if } |S_{faul\,2}| < |S_{faul\,1}| \tag{2.9}$$

where $S_{fault\,1}$ and $S_{fault\,2}$ indicate the sets of signals affected by variations due to the abnormal (faulty) conditions, and $|S_{faul\,1}|$ and $|S_{faul\,2}|$ their cardinality. If it is considered, for example, the problem of sensor failures, it is reasonable to assume that the probability of having N_1 faulty sensors at the same time is lower than that of having an higher number of faulty sensors, $N_2 < N_1$, at the same time. This situation is outlined in Fig. 2.3, where the historical observations representing the component behavior in normal conditions are represented by dots and the abnormal condition test pattern by a square. According to the assumption in eq. (2.9), it is more probable that the abnormal condition is caused by a failure of a single component (for example, corresponding to normal conditions close to the pattern in **B**) than by a simultaneous failure of two components (corresponding to normal conditions close to the pattern in **A**).

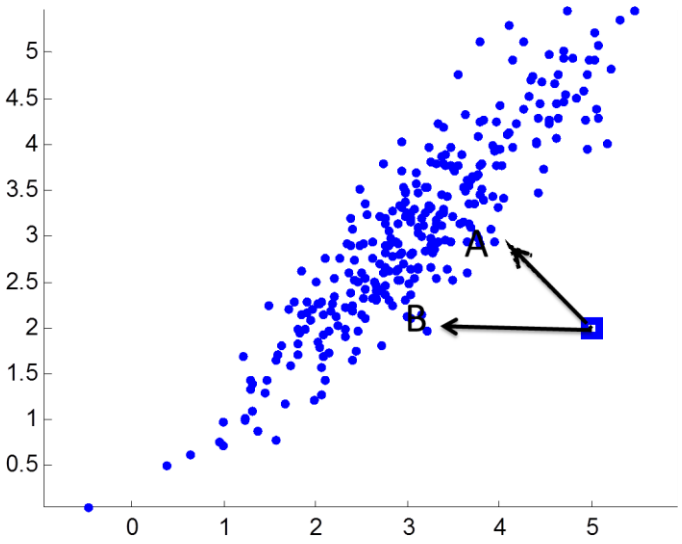

Fig. 2.3 Set of high correlated historical observations (dots) and test pattern (square). A represents the possible reconstruction of the test pattern in the case in which only one component is faulty, B is the case in which 2 components are faulty.

The proposed procedure computes the similarity measure between the observation, $\vec{x}^{obs}$, and the generic k-th historical observation, $\vec{x}^{obs-nc}(k)$, according to two steps: (a) a pre-processing step consisting in the projection of $\vec{x}^{obs}$ and $\vec{x}^{obs-nc}(k)$ in a new space defined by a penalization vector, $\vec{p} = [p(1), \dots, p(J)]$, with increasing entries, i.e., $p(1) < \cdots < p(J)$ and (b) the application of the Gaussian RBF kernel in the new space.

Step (a) is based on:

- computing the vector of the absolute values of the normalized differences between $\vec{x}^{obs}$ and $\vec{x}^{obs-nc}(k)$:

$$\left|\vec{x}^{obs} - \vec{x}^{obs-nc}(k)\right|_{\sigma} = \\ = \left(\left|\frac{\vec{x}^{obs}(1) - \vec{x}^{obs-nc}(k,1)}{\sigma_1}\right|, \dots, \left|\frac{\vec{x}^{obs}(J) - \vec{x}^{obs-nc}(k,J)}{\sigma_J}\right|\right) \quad (2.10)$$

- defining a permutation matrix, P_{perm}, i.e. a matrix which, when multiplied to a vector, only modifies the order of the vector components; in our procedure, we define a matrix, P_{perm}, such that when it is applied to the vector $|\vec{x}^{obs} - \vec{x}^{obs-nc}(k)|_{\sigma}$, the components of the obtained vector are the same of that of $|\vec{x}^{obs} - \vec{x}^{obs-nc}(k)|_{\sigma}$, but they appear in a decreasing order, i.e.

the first component is the one with the largest difference in $|\vec{x}^{obs} - \vec{x}^{obs-nc}(k)|_{\sigma}$;

- defining a diagonal matrix having decreasing entries on its diagonal:

$$D_{\vec{p}} = \begin{bmatrix} \sqrt{p(1)} & 0 & 0 \\ 0 & \ddots & 0 \\ 0 & 0 & \sqrt{p(J)} \end{bmatrix} \tag{2.11}$$

where the vector $\vec{p} = [p(1), \dots, p(J)] = tr(D_{\vec{p}})$ will be referred to as penalization vector;

- projecting $\vec{x}^{obs}$ and $\vec{x}^{obs-nc}(k)$ in a new space defined by the transformation:

$$\begin{aligned} \boldsymbol{\psi} &: \mathbb{R}^J \rightarrow \mathbb{R}^J \\ \boldsymbol{\psi}(\vec{x}^{obs}) &= D_{\vec{p}}\, P_{perm}\, \vec{x}^{obs} \\ \boldsymbol{\psi}(\vec{x}^{obs-nc}) &= D_{\vec{p}}\, P_{perm}\, \vec{x}^{obs-nc} \end{aligned} \tag{2.12}$$

In step (b), we apply to $\boldsymbol{\psi}(\vec{x}^{obs})$ and $\boldsymbol{\psi}(\vec{x}^{obs-nc})$ the Gaussian kernel with Euclidean distance:

$$w(k) = Ker\left(\boldsymbol{\psi}(\vec{x}^{obs}), \boldsymbol{\psi}(\vec{x}^{obs-nc})\right) = \frac{1}{\sqrt{2\pi h^2}} e^{-\frac{\left\|\boldsymbol{\psi}(\vec{x}^{obs}) - \boldsymbol{\psi}(\vec{x}^{obs-nc})\right\|^2}{2h^2}} \tag{2.13}$$

Notice that in this work it is not investigated whether the sequential application of steps (a) and (b) defines a kernel function according to eq. (2.3). Here, in order to show the effects of its application, two different historical patterns, $\vec{x}^{obs-nc}(k_1)$ and $\vec{x}^{obs-nc}(k_2)$, are considered, which are characterized by similar Euclidean distance from a test pattern, but with $\vec{x}^{obs-nc}(k_1)$ characterized by a lower number of signals remarkably different from that of the test pattern. In this case, the effect of the penalty vector is to assign to $\vec{x}^{obs-nc}(k_1)$ an higher similarity measure than that assigned to $\vec{x}^{obs-nc}(k_2)$. Considering the case of Fig. 2.3, the similarity of $\vec{x}^{obs}$ (square) with the pattern in **B** results higher than that with the pattern in **A**, whereas, according to the traditional AAKR pattern **A** is more similar than pattern **B** to the test pattern.

Fig. 2.4 shows the locus of points characterized by the same similarity to the origin (0,0) in a 2-dimensional space using a penalty vector $\vec{p} = [1, 30]$. The

obtained surface is very different from the circle which would be obtained by using an Euclidean distance. As expected, such modification introduces a preference during the reconstruction of $\vec{x}^{obs}$ for that points of $\bar{\bar{X}}^{obs-nc}$ that have deviation on a lower number of components.

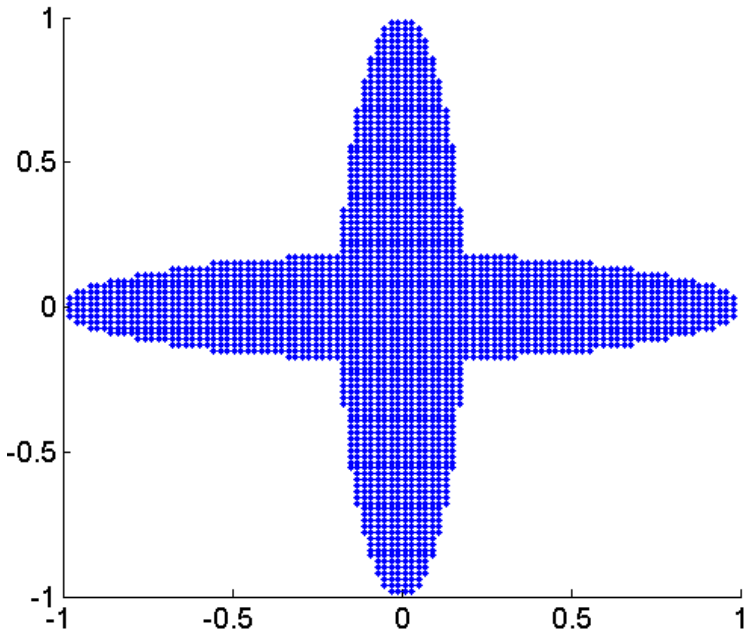

Fig. 2.4 2D locus of points having similarity from the origin greater than a set value according to a penalty vector $\vec{p} = [1\ 30]$

The application of the proposed method is also exemplified with reference to a numerical conceptual case study. Let us assume to have available an infinite dataset of historical data containing all the possible normal conditions of 3 signals with degree of correlation equal to 1, i.e. ($\vec{x}^{obs-nc}(k) = [k, k, k] \in \mathbb{R}^3$, $k \in (-2,2)$) and to have a test pattern $\vec{x}^{obs} = [1,0,0]$ containing the three signal measurements at the present time. According to the traditional AAKR procedure, the Euclidean distance between the test pattern and the k-th training patterns is: $d^2(k) = (k-1)^2 + k^2 + k^2$, which leads to identifying the historical pattern $\vec{x}_{nearest\_eucl} = \left[\frac{1}{3}, \frac{1}{3}, \frac{1}{3}\right]$ as the nearest to the test pattern (see Fig. 2.5 and Fig. 2.6). Thus, $\vec{x}_{nearest\_eucl}$ will be associated to the highest weight, and the signal reconstruction will be close to it. The reconstruction suggests that there is an abnormal condition impacting all three signals at the same time. Let us now consider the reconstruction performed by using the proposed method with a penalization vector $\vec{p} = [1, 10, 100]$. In this case, the most similar pattern is

$\vec{x}_{nearest\_pen} = \left[\frac{1}{111}, \frac{1}{111}, \frac{1}{111}\right]$ and the signal reconstruction will be close to it. Hence, according to this approach, the only significant residual is detected on the first signal (Fig. 2.5 and Fig. 2.6).

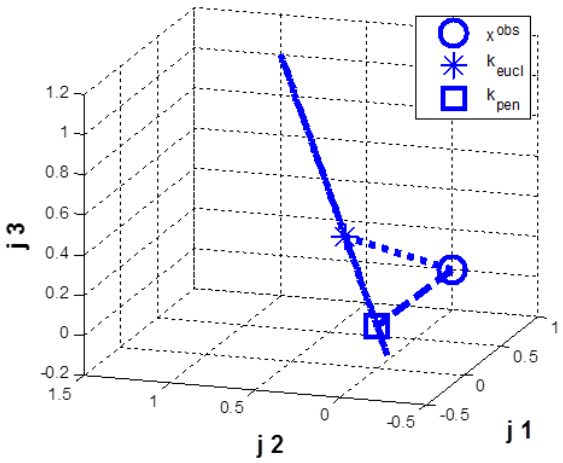

Fig. 2.5 Reconstruction of an abnormal condition (circle) performed with the Euclidean AAKR (star) and the penalty AAKR (squared).

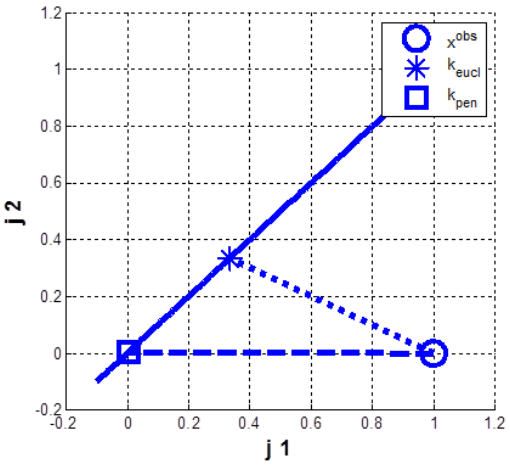

Fig. 2.6 Projection of the reconstruction on the plain described by two signals.

Notice that the basic difference between the reconstructions provided by the traditional and the modified AAKR algorithm is the hypothesis of the latter that an abnormal condition involving few signals is more probable than an abnormal condition involving a lot of signals. Coherently with that hypothesis, the modified AAKR identifies an abnormal behavior only on one signal.

2.5 Case Study: Industrial Components

The data previously introduced in Section 2.3 are used to test the performance of the proposed modified AAKR method. The dataset which contains the measurements of 6 highly correlated signals in 5200 time steps has been divided into 3 subsets:

- Training set $\bar{\bar{X}}_{train}^{obs-nc} \in \mathbb{R}^{2500 \times 6}$, used as historical dataset to perform the reconstruction;
- Validation set $\bar{\bar{X}}_{val}^{obs-nc} \in \mathbb{R}^{1700 \times 6}$, used for the setting of the optimal parameter values;

- Test set, $\bar{\bar{X}}_{test}^{obs-nc} \in \mathbb{R}^{1000 \times 6}$, used for testing the performance of the method.

In order to verify the performance of the proposed method in case of abnormal conditions, sensors failures have been simulated in the test set. In practice, assuming that sensor failures are independent events with probability, q (e.g. q=0.2), the following procedure has been applied:

- for each signal and each test pattern, a random number, r, has been sampled from an uniform distribution in [0,1]. If $r < q$, the sensor is assumed to be failed and a deviation is simulated from a bimodal uniform distribution $U([-10,-4] \cup [4,10])$ and added to the sensor measurement.

Thus, the number of signals affected by a deviation in each test pattern is distributed according to a Binomial distribution $B(q,6)$. The deviation intensity has been sampled from the uniform distribution $U([-10,-4] \cup [4,10])$ in order to avoid to confuse the added deviations with the measurement noise which has been estimated to be a Gaussian noise with standard deviation equal to 1.5.

The obtained test set, $\bar{\bar{X}}_{err}$, containing both normal and abnormal conditions patterns, $\vec{x}_{err}(k)$, has been used to verify the performance of the traditional AAKR method and the modified AAKR with different choices of penalization vector:

- Linear $\vec{p} = [m, 2m, \dots, 6m]$, with $m \in \{2, 4, 8, 16, 32, 64\}$;
- Exponential $\vec{p} = [\kappa, \kappa^2, \dots, \kappa^6]$, with $\kappa \in \{2, 5, 10, 15, 20\}$;
- Cliff Diving Competition ranking $\vec{p} = [8\ 20\ 50\ 90\ 160\ 350]$.

In all cases, the optimal bandwidth parameter, h, has been identified by minimizing the Mean Square Error (MSE) of the reconstructions on the validation set, $\bar{\bar{X}}_{val}^{obs-nc}$:

$$MSE(h) = \frac{\sum_{k=1}^{N_{val}} \sum_{s=1}^{J} \left(\hat{\bar{x}}_{val}(k,s) - \vec{x}_{val}^{obs-nc}(k,s) \right)^2}{N_{val}} \tag{2.14}$$

Then, for each test pattern, $\vec{x}_{err}(k)$, of $\bar{\bar{X}}_{err}$, with $k = 1, \ldots, 1000$, the reconstruction $\hat{\vec{x}}_{nc}(k)$ of the signals values expected in normal conditions has been performed, and the residuals $\hat{\vec{r}}(k)$ computed. Finally, if $\hat{r}(k,j) > 4$, for $j = 1, \ldots, 6$, an abnormal condition involving signal j is detected.

In order to evaluate the performance in the reconstruction, notice that 4 different possible cases for each test pattern are considered:

1) presence of both false and missed alarms. There is at least one signal for which an abnormal condition is erroneously detected ($\hat{r}(k,j) > 4$) when no sensor failure has been simulated (false alarm) and, at the same time, at least one signal for which an abnormal condition is erroneously not detected ($\hat{r}(k,j) < 4$), when actually a sensor failure has been simulated (missed alarm);
2) presence of only a false alarm. At least one false alarm, no missing alarms;
3) presence of only a missed alarm. At least one missed alarm, no false alarms;
4) correct identification (OK). Neither false nor missing alarms.

Table 2.2 reports the performance of the traditional and modified AAKR reconstruction methods in terms of fraction of test patterns in which the application of the detection scheme leads to one of the four categories (1-4), considering different choices of the penalization vector. For the cases of exponential and linear penalization vectors, only the results obtained for k=10 and m=8, which correspond to the best performance, are reported.

	PENALIZATION VECTOR	**OK**	**MISSED ALARMS**	**FALSE ALRAMS**	**MISSED AND FALSE ALARMS**
MODIFIED AAKR	**EXPONENTIAL κ = 10**	0.885	0.089	0.008	0.018
MODIFIED AAKR	**DIVING COMPETITION RANKING**	0.669	0.300	0.001	0.030
MODIFIED AAKR	**LINEAR m = 8**	0.585	0.375	0.001	0.039

TRADITIONAL AAKR	**EXPONENTIAL κ = 1**	0.500	0.446	0.003	0.051

Table 2.2 Fraction of test patterns correctly identified (OK), missed, false and both missed and false alarms

The most satisfactory method from the point of view of the highest fraction of correct identification and the lowest fraction of missed and false alarms is the modified AAKR with an exponential penalty vector, whereas the less satisfactory is the traditional AAKR. Furthermore, notice that the lowest total fraction of false alarms, which can be obtained from the sum of the false and false and missed alarms (columns 5 and 6 of Table 2.2), is obtained by the modified AAKR with exponential weight vector.

The performance of the modified AAKR method with exponential penalty vector and k=10 has also been verified on the same case study considered in in Section 2.3 (Fig. 2.2) characterized by a linearly increasing drift on one signal. Fig. 2.7 and Fig. 2.8 shows another signal not affected by failure. Notice that the modified AAKR provides an early detection of the abnormal conditions, with the obtained residuals almost overlapping the simulated drift. Furthermore, the reconstruction of the signal not affected by the drift is very accurate with residuals close to 0. Hence, the modified AAKR allows to reduce the time necessary for the sensor failure detection with respect to the traditional AAKR and is more resistant to the spill-over effect.

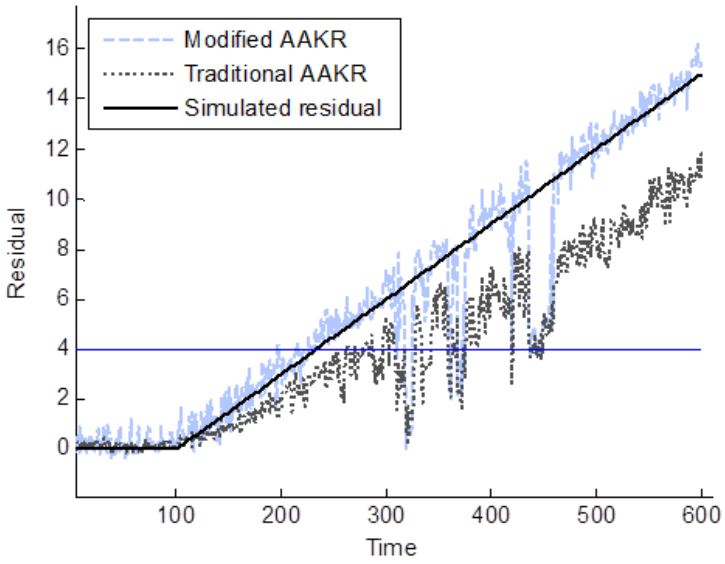

Fig. 2.7 Residual of the drifted signal

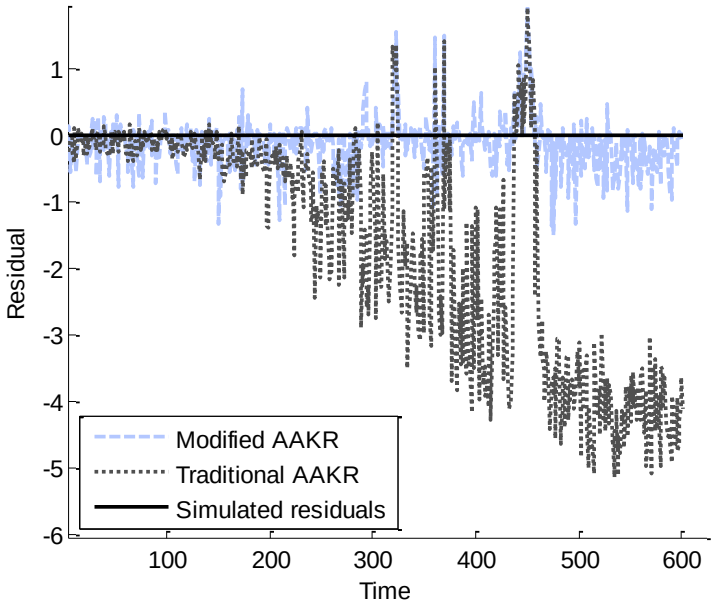

Fig. 2.8 Residual of a signal not affected by any drift

Further analyses have been performed in order to identify the sensitivity of the modified AAKR method to the setting of the exponential penalty vector parameter, to the number of simultaneous sensor failures and to the intensity of the failure.

With respect to the setting of the parameter κ of the exponential penalty vector, Fig. 2.9 reports the fault detection performance obtained by varying its value. Notice that for κ=1 the modified AAKR method becomes the traditional AAKR method, and, thus, its performance, as reported in Table 2.2, is less satisfactory. Values of $\kappa \geq 20$ are associated to an increasing percentage of false and missing alarms since the method tends to identify failures on healthy sensors. It is, however, interesting to note that the performance is not very sensitive to variation of κ in the range of $\kappa = [10,40]$, where the percentage of correct detection remains larger than 90% and the percentage of false and false and missed alarms are subject to small variations.

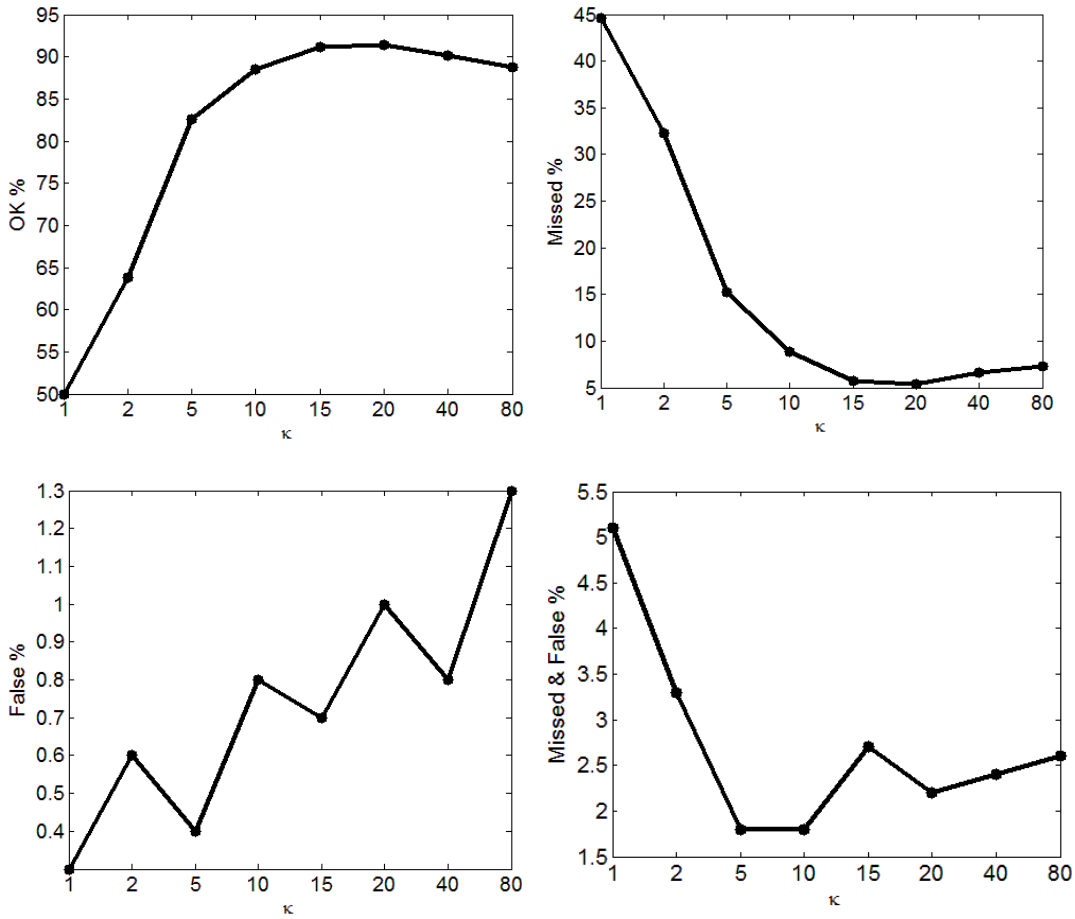

Fig. 2.9 Sensitivity to the parameter κ defining the exponential penalty vector: top-left) correct detection; top-right) missed alarms; bottom-left) false alarms; bottom-right) missed and false alarms

In order to assess the performance of the method considering different numbers of simultaneous sensor failures, we have simulated 2 new test datasets of 1000 patterns each one obtained by adding deviations on 2 and 4 signals to the

normal condition measurements, respectively. The obtained results are reported in Table 2.3. The modified AAKR method tends to perform remarkably better than the traditional AAKR method in the cases of two simultaneous sensor failures. However, the performance of the two methods tends to decrease if the number of simultaneous sensor failures increases. In particular, in the case of four simultaneous sensor failures, the traditional AAKR method performance is slightly more satisfactory than that of the modified method. This is due to the consequences of the modified AAKR method hypothesis that signal behaviors characterized by several signals affected by abnormal conditions are expected to be rare and so the number of missed alarms increases. This can be explained by considering the same numerical conceptual case study discussed in Section 2.3. Let us assume that we have to reconstruct the test pattern $\vec{x}^{obs} = [1,1,0]$ which is characterized by a failure of sensors 1 and 2 (normal condition measurements would be $[0,0,0]$). Considering a training set made of patterns ($\vec{x}^{obs-nc}(k) = [k,k,k] \in \mathbb{R}^3,\ k \in (-2,2)$), the traditional AAKR reconstructs the test pattern in the neighborhood of $\left[\frac{2}{3},\frac{2}{3},\frac{2}{3}\right]$, which is the closest training pattern using an Euclidean distance, whereas the modified AAKR with penalty vector $\vec{p} = [1,10,100]$ reconstructs it in the neighborhood of $\left[\frac{110}{111},\frac{110}{111},\frac{110}{111}\right]$. Hence, the traditional AAKR method detects an anomaly on all the three sensors, providing a false alarm on sensor 3, whereas the modified AAKR detects a failure on sensor 1, providing a false alarm on sensor 1 and missed alarms on sensors 2 and 3. In general, it seems that the performance of the modified AAKR is satisfactory when the total number of sensor failures is lower than half of the number of sensors $\left|S_{fauls}\right| \leq \frac{|S_{tot}|}{2}$].

	2 Simultaneous Errors			
	OK	**MISSED**	**FALSE**	**MISSED & FALSE**
Traditional AAKR	335	577	9	79
Exponential κ = 10	837	158	2	3

Table 2.3 Quantitative results for 2 simultaneous error

	4 Simultaneous Errors			
	OK	**MISSED**	**FALSE**	**MISSED & FALSE**
Traditional AAKR	170	637	16	177
Exponential κ = 10	38	302	87	573

Table 2.4 Quantitative results for 4 simultaneous error

The sensitivity of the method to the intensity of the deviations has been investigated by adding to the signals of the dataset $\bar{\bar{X}}_{err}$ deviations of intensity sampled uniformly in the interval [9,10] instead of [4,10]. The results reported in Table 2.5 shows that:

- the number of correct detections performed by the traditional AAKR method increases due to the decrease of the number of missed alarms;
- both the numbers of *false alarms* and *missed and false alarms* increase due to the spill-over effect on the remaining signals.

With respect to the modified AAKR method, in case of higher intensity of the deviations, the number of missed alarms decreases, whereas the increase of the number of false alarm is lower than that of the traditional AAKR. This confirms that the modified AAKR is more resistant to spill-over than the traditional AAKR.

		OK	**MISSED**	**FALSE**	**MISSED & FALSE**
κ = 10	**E_i ~ U([4, 10])**	887	85	10	18
	E_i ~ U([9, 10])	936	2	26	36
κ = 1	**E_i ~ U([4, 10])**	489	440	7	64
	E_i ~ U([9, 10])	757	64	70	109

Table 2.5 Quantitative detection results with increasing deviation intensity for the Euclidean AAKR $\kappa = 1$ and for the penalized AAKR $\kappa = 10$

2.6 Conclusion

In this chapter, the condition monitoring of an industrial component has been considered within a data-driven setting. In order to obtain robust reconstructions of the values of the monitored signals expected in normal conditions, it has been proposed to modify the traditional AAKR method. The modification is based on a different procedure for the computation of the similarity between the present and the historical measurements collected in normal condition of operation. In particular, before the computation of the Kernel between the two vectors, which is performed as in the traditional AAKR method according to a Gaussian RBF function, the data are projected into a new signal space defined by using a penalization vector which reduces the contribution of signals affected by malfunctioning. The procedure is based on the hypothesis that the probability of occurrence of a fault causing variations on a large number of signals is lower than that of one causing variations on a small number of signals.

The modified AAKR method has been applied to a real case study concerning the monitoring of 6 highly correlated signals in an industrial plant for energy production. The possibility of detecting sensor faults has been investigated. The obtained results have shown that the reconstructions provided by the modified AAKR are more robust than those obtained by using the traditional AAKR. This causes a reduction in the time necessary to detect abnormal conditions and in a more accurate identification of the signals actually affected by the abnormal conditions.

3

Bayesian Filter-Based Fault Detection

With regards to the model-based approaches, a number of filtering algorithms have been successfully applied to FDI, which use discretized differential equations to describe the state evolution, and stochastic noises to take into account the associated aleatory uncertainty([6], [30], [36], [37] and [47]). However the high complexity of real industrial system demand for method capable of manage nonlinear non-Gaussian models, since there are still situations where traditional filtering techniques fail. In this context, Particle Filtering (PF) has proven to be a robust technique ([2],[17]) which allows tackling more realistic FDI problems([46],[49] and [50]). In particular, PF has been adopted as a FDI tool within the Multi-Model (MM) systems framework, where the description of the possible abnormal evolutions of the component behavior relies on a set of models [31]. In this setting, detection aims at identifying when the behavior of the component starts to leave the nominal mode, whereas diagnostics consists in selecting the model that best fits in describing the current behavior of the component.

Interesting applications of PF to FDI in MM systems have been proposed in [1] and [12], where multiple swarms of particles are contemporaneously simulated, according to all the possible alternative models. There, FDI are based on Log-

Likelihood Ratio (LLR) tests, which exploit the gathered measures to estimate, for every swarm, the corresponding likelihood of being the right model to track the observed component behavior. However, these methods are computationally burdensome and memory demanding, as they require tracing a large number of particles.

Alternatively, an approach based on the augmentation of the state vector with a variable representing the model to be selected to describe the current evolution has been propounded in [39] and [42]. This allows the filter to automatically convey the particles to follow the right model when the gathered measures force the state vector to modify the value of the added variable.

In particular, such variable is chosen continuous in [32], which proposes an ensemble of Monte Carlo adaptive filters, and uses the LLR tests to make the FDI decision. On the contrary, it is a Boolean variable in [39] and [46], where explicit fault models with associated fault probabilities are supposed to be known. These are used to compel the particles to evolve according to the different models. Then, the measures acquired at the updating steps will favor the particles of the correct model, i.e., those associated to the correct value of the added variable, which are expected to be more close to the measured degradation value.

On the other side, the works of the literature which investigate the potential of such algorithm ([39] and [46]) addressed case studies where only two models are available, the noise is Gaussian, and the occurrence of a fault reflects in a sharp jump of the traced degradation variable. These hypotheses may be unrealistic, especially for continuously degrading components [14]. In this context, the novelty introduced in this chapter, is to apply PF to FDI in MM systems where more than two models are available, the noise in the models is not Gaussian and the degradation process are smoothly evolving. The performances of the proposed approach are compared with those of both the LLR-based approach (e.g. [12]), and an intuitive approach based on the statistical hypothesis test technique.

To this aim, a non-linear crack growth degradation process is considered as case study, which is investigated in two different settings:

1) There are only two models available, one for normal conditions and the other for degradation; hence, detection and diagnosis coincide. This is the same setting of other works of the literature (e.g. [39], [46])
2) A third degradation model is considered, in order to evaluate the diagnostic capability of the proposed approach in selecting the right model to describe the current evolution behavior.

The remainder of the chapter is organized as follows. In Section 3.1, a general description of the Multi Model setting is presented, with a focus on the case study considered in this chapter. In Section 3.2, basics of Particle Filtering are recalled. Section 3.3 summarizes the characteristics of the PF-based techniques proposed in the literature to address FDI in Multi Model systems, and describes the FDI technique based on the augmented state vector. Section 3.4 shows the application of these FDI methods to the simulated realistic case study of the crack growth degradation process. Section 3.5 reports some conclusions.

3.1 Multi Model System

The evolution of a Multi Model system cannot be described by the same model during its entire life cycle, but requires a set of *M* models, each one capturing different behaviors of the systems in different situations or phases. Thus, a set of *M* state equations are proposed to describe the possible system functioning conditions, which are usually divided into two main classes:

N models for normal conditions $m_{n_1}, \dots, m_{n_N}$:

$$\begin{aligned} m_{n_1}&: \boldsymbol{x}_k = \boldsymbol{f}_{k-1}^{n_1}\left(\boldsymbol{x}_{k-1}, \boldsymbol{\omega}_{k-1}^{n_1}\right) \\ &\dots \\ m_{n_N}&: \boldsymbol{x}_k = \boldsymbol{f}_{k-1}^{n_N}\left(\boldsymbol{x}_{k-1}, \boldsymbol{\omega}_{k-1}^{n_N}\right) \end{aligned} \tag{3.1}$$

F models for fault conditions $m_{f_1}, \dots, m_{f_F}$:

$$\begin{aligned} m_{f_1}&: \boldsymbol{x}_k = \boldsymbol{f}_{k-1}^{f_1}\left(\boldsymbol{x}_{k-1}, \boldsymbol{\omega}_{k-1}^{f_1}\right) \\ &\dots \\ m_{f_F}&: \boldsymbol{x}_k = \boldsymbol{f}_{k-1}^{f_F}\left(\boldsymbol{x}_{k-1}, \boldsymbol{\omega}_{k-1}^{f_F}\right) \end{aligned} \tag{3.1}$$

where *N*+*F*=*M*, $\boldsymbol{x_k}$ represents the state vector at time t_k, and $\boldsymbol{\omega}_{k-1}$ is the noise at the previous time step, t_{k-1}, which defines the aleatory uncertainty in the evolution of the process.

A further assumption made when MM systems are considered is that the state $\boldsymbol{x}_k$ cannot be precisely measured, and the knowledge about its value is affected by uncertainty, represented by the noise $\boldsymbol{\nu}_k$**.** The measurement model:

$$\boldsymbol{y}_k = \boldsymbol{g}_k(\boldsymbol{x}_k, \boldsymbol{\nu}_k) \tag{3.2}$$

that links the state $\boldsymbol{x}_k$ to the measurement acquired $\boldsymbol{y}_k$ is supposed to be given.

In this work, we consider a fatigue crack growth degradation process in a mechanical component (Fig. 3.1), which is a typical example of MM system, is considered. Degradation evolution is divided into three phases [22]:

- Incubation; it is the short initial phase of the phenomenon, which is connected with plastic strains locally occurring in the most stressed parts

of the mechanical component subject to cyclic loads. At this stage, coalescence of dislocations and vacancies, as well as ruptures due to local stresses lead to the formation of sub-microcracks in the slip bands at the boundaries of blocks, grains and twins. From the practical point of view, this phase is modeled by a constant model in which the crack length is zero, being its exact value not measurable by traditional measurement instrumentation.

- Crack initiation; it is characterized by the growth and coalescence of the sub-microcracks, which transform into micro-cracks. These start increasing under the cyclic loads, and form macro-cracks, which are typically detectable by measurement instrumentation. This gives rise to the third phase. The model describing this second phase is linear in time [9].
- Crack rapid-propagation; the crack grows under the cyclic loads, up reaching a critical threshold. A number of models have been proposed to describe this latter phase, such as the Paris-Erdogan exponential law [40], here considered.

The measures gathered to monitor the degradation process are affected by errors, especially during the second phase or when the crack cannot be directly measured due to its position. In this setting, detection consists in the identification of the deviation from the first phase, while diagnostics consists in determining whether the growth is linear (i.e., the second phase) or exponential (i.e., the third phase).

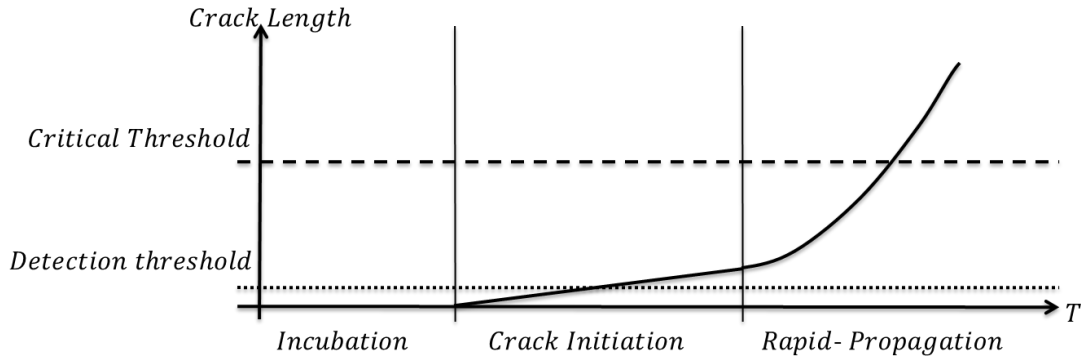

Fig. 3.1 Schematic approximation of the crack propagation model.

3.2 Particle Filtering

Particle Filtering (PF) is a sequential Monte-Carlo method, which is made up of two subsequent steps: prediction and updating. At time t_{k-1}, the prediction of the equipment state $\boldsymbol{x}_k$ at the next time instant t_k, is performed by considering a set of N_S weighted particles, which evolve independently on each other, according to the given probabilistic degradation model (i.e., one out of those in Eqs. (3.1)). The underlying idea is that such group of weighted random samples provides an empirical discrete approximation of the true Probability Density Function (pdf) $P(\boldsymbol{x}_k|\boldsymbol{y}_{k-1})$ of the system state $\boldsymbol{x}_k$ conditional on the last available measure. When a new measure $\boldsymbol{y}_k$ is acquired, it is used to update the proposed pdf in a Bayesian prospective, by adjusting the weights of the particles on the basis of their likelihood of being the correct value of the system state. For practical purpose, PF works as if the *i*-th particle, *i*=1, 2, …N_S were the real system state; then, the smaller the probability of observing the last collected measurement, the larger the reduction in the particle's weight. On the contrary, when the acquired measure well matches with the particle position, then its importance is increased. Such updating step of the particle weights is driven by the probability distribution $P(\boldsymbol{y_k}|\boldsymbol{x_k})$ (which is derived from Eq. (3.2)) of observing the sensors output $\boldsymbol{y_k}$ given the true degradation state $\boldsymbol{x}_k$, and provides the distribution $P(\boldsymbol{x_k}|\boldsymbol{y_k})$.

The PF scheme used in this work is the Sequential Importance Resampling (SIR, , [2], [17]), which builds a new population of particles by sampling with replacement from the set of particles $\{\boldsymbol{x}_k^1, \dots, \boldsymbol{x}_k^{N_S}\}$; the chance of a particle being picked is proportional to its weight. The final weight assigned to the particles of such new set is $\frac{1}{N_S}$. The SIR algorithm allows avoiding the degeneracy phenomenon (i.e., after few iterations, all but few particles would have negligible weights), which is typical of the standard version of PF (i.e., Sequential Importance Sampling, SIS).

Finally, the updated particle distribution is used to perform the successive prediction steps up to next measurement (for further theoretical details see [2], [17], [18] and [34]).

3.3 Particle Filter for Fault Detection and Diagnosis in Multi Model System.

PF has been already applied to tackle FDI issues in the framework of MM systems. For example, in [31] PF is used to simultaneously run swarms of particles evolving according to every possible model (Fig. 3.2). Then, a residual's analysis or a Log-Likelihood Ratio (LLR) test is performed to identify the swarm that best matches with the gathered measure, and thus the corresponding model. For example, Fig. 3.2 shows the case in which three different swarms are traced by PF, according to three available models m_n, m_{f1} and m_{f2}. Model m_n is the best model to represent the system evolution in its first phase, being very good the matching of the corresponding particle swarm and the measures acquired at time instants T_1, T_2, T_3. On the contrary at time T_5 the model which best fits the measures becomes m_{f2}.

Enhancements of this approach have been proposed in [1] and [12]. In the former work, a new way to estimate the likelihood function is introduced to extend the applicability of the method to more complex particle distributions. In

the latter, a swarm of particles for every possible evolving model is created at every time step, and traced to detect the occurrence of a fault at any subsequent time instant. For example, Fig. 3.3 shows that two new swarms are created at every measurement step, which evolve according to models m_{f1} and m_{f2}, alternative to m_n. The presence of diverse swarms increases the promptness in detecting the change in the behavior of the system, which is again established by LLR tests. On the other side, this advantage is counterbalanced by the onerous computational time due to the large number of particles to be simultaneously traced. To partially overcome this problem, the authors in [12] proposed to consider an observation window, at whose end the swarms are no longer traced. Obviously, the width of such time window needs to be set large enough to allow the LLR to robustly detect model changes. Then, this approach is not effective when the models need a long transition time to significantly diverge, as this would require fixing wide observation windows. Furthermore, the number of particles to be drawn raises with the number of system's models.

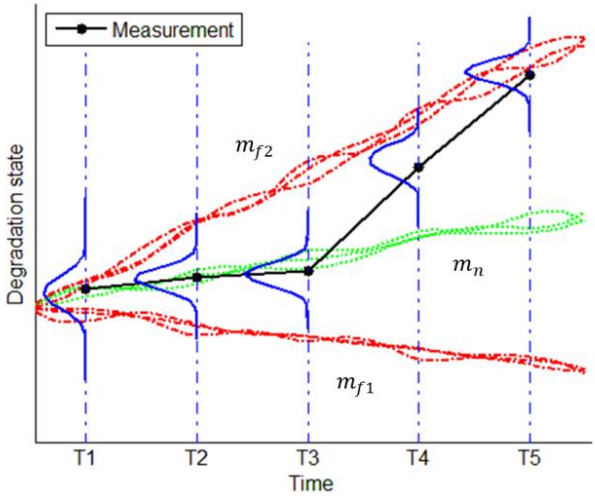

Fig. 3.2 Parallel swarms of particles evolve according to the available models. At every T_k, particle weights are updated driven by $p(y_k|x_k)$.

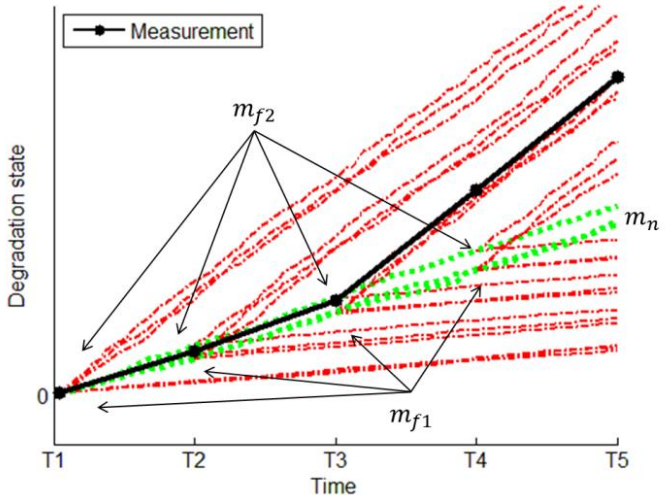

Fig. 3.3 At every time step, new swarms of particles start according to the alternative models.

A different way to tackle the MM problems is that of augmenting the state vector with a new discrete variable, which represents the evolution model of the system. That is, the state vector becomes $\boldsymbol{x'_k} = [\boldsymbol{x_k}\ \theta_k]^T$, and the degradation models in eq. (3.1) are embedded in the model:

$$\boldsymbol{x'_k} = f'(\boldsymbol{x'_{k-1}}, \boldsymbol{\omega}_{k-1,\theta_{k-1}}) = f'(\boldsymbol{x_{k-1}}, \theta_{k-1}, \boldsymbol{\omega}_{k-1,\theta_{k-1}}) \tag{3.3}$$

where f' encodes also the probabilistic model governing the transitions among the different possible models, which is a first-order Markov [46].

This setting requires modifications to the PF algorithm. In details, the PF prediction step has to give due account to the possible alternative models according to which the particles are simulated:

$$\begin{aligned} p(\boldsymbol{x'_k}|\,\boldsymbol{y}_{k-1}) &= \int p(\boldsymbol{x'_k}|\boldsymbol{x'_{k-1}})p(\boldsymbol{x'_{k-1}}|\,\boldsymbol{y}_{k-1})d\boldsymbol{x'_{k-1}} = \\ \int \sum_{\theta_{k-1}} p(\boldsymbol{x}_k, \theta_k|\boldsymbol{x}_{k-1}, \theta_{k-1})p(\boldsymbol{x}_{k-1}, \theta_{k-1}|\,\boldsymbol{y}_{k-1})\,d\boldsymbol{x}_{k-1} &= \\ = \int \sum_{\theta_{k-1}} p(\boldsymbol{x}_k|\boldsymbol{x}_{k-1}, \theta_k)p(\theta_k|\,\theta_{k-1})p(\boldsymbol{x}_{k-1}, \theta_{k-1}|\,\boldsymbol{y}_{k-1})d\boldsymbol{x}_{k-1} & \end{aligned} \tag{3.4}$$

In the last equation, it has been assumed that the transition probabilities $p(\theta_k \mid \theta_{k-1})$ do not depend on the current degradation state $\boldsymbol{x}_{k-1}$, whereas the prediction of the state $\boldsymbol{x}_k$ depends on the added variable θ_k, whose value is sampled at the current time instant t_{k-1}.

The successive updating step at time t_k acts on the distribution of $\boldsymbol{x}_k$ only, since the acquired measures concern the value of the degradation state $\boldsymbol{x}_k$, and not that of the variable θ_k. Nonetheless, favoring the particles positioned in the neighborhood of the measure $\boldsymbol{y}_k$ leads to the selection of the particles with the most likely value of θ_k.

For the sake of clarity, the transition probabilities $p(\theta_k \mid \theta_{k-1})$ in (3.4) can be arranged in the matrix:

$$A_{trans} = \begin{bmatrix} A_{11} & A_{12} & \dots & A_{1M} \\ A_{21} & A_{22} & \dots & A_{2M} \\ \dots & \dots & \dots & \dots \\ A_{M1} & A_{M2} & \dots & A_{MM} \end{bmatrix} : A_{ij} \geq 0, \forall\, i,j = 1,2,\dots M \tag{3.5}$$

where the *i*-th element of the *j*-th column represents the probability that a particle which has been simulated according to model *i*, will be simulated at the next step according to model *j*.

For example, in the case in which there are *M*=2 alternative models, model 1 refers to the normal state (*N*=1), whereas model 2 to the failed state (*F*=1). Then, A_{11} is the probability that a particle which at the previous step has been simulated according to model 1, will be simulated again according to the same model 1, whereas A_{12} is the opposite case, i.e., the same particle will change its stochastic behavior. Fig. 3.4 gives a pictorial view of this dynamics.

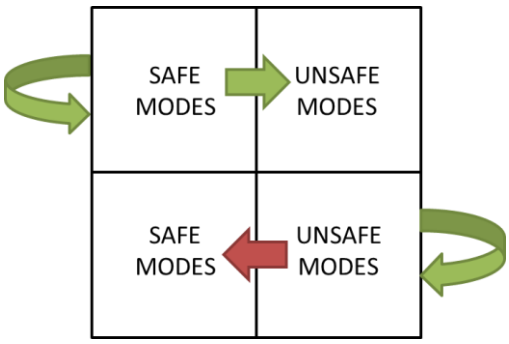

Fig. 3.4 Possible transitions among the operational models of the system.

Notice that the transition from model j to model i, $j > i$, may be physically meaningless when it is not possible that a system spontaneously recovers by itself. However, in the considered setting a positive value is always given to the corresponding probabilities. In fact, if these were set to zero, the system would be biased to follow the degraded models especially in case of outlier measure

values, as the trajectories of those particles that are erroneously following a failure model could no longer be corrected.

For the sake of clarity, an example of the dynamic behaviors of the particles when the measures are gathered from the normal operating system is given in Fig. 3.5. At time t_0, some particles change their reference model according to A_{trans}. In particular, some particles experienced a change of the variable θ_k from θ_N to θ_F. These particles are strongly un-favored at the updating step, being the acquired measure far from their positions. Thus, among the particles with state parameter θ_F, only few particles (one in Fig. 3.5) are re-sampled and still follow the wrong model at the next time step, whereas the others are reset to the starting point. The behavior of the augmented MM PF in the opposite case, i.e., when measurements are gathered from a failed system, is shown in Fig. 3.6. There, during the updating and re-sampling steps, the number of particles having θ_F as augmented state increases. Hence, the measures acquired promote the particles associated to the correct model, i.e., those labeled with the correct value θ_F of the added variable, which are more close to the measured degradation value. This allows the particles to auto-adapt their trajectories to the real evolution of the system, and thus selecting the correct model.

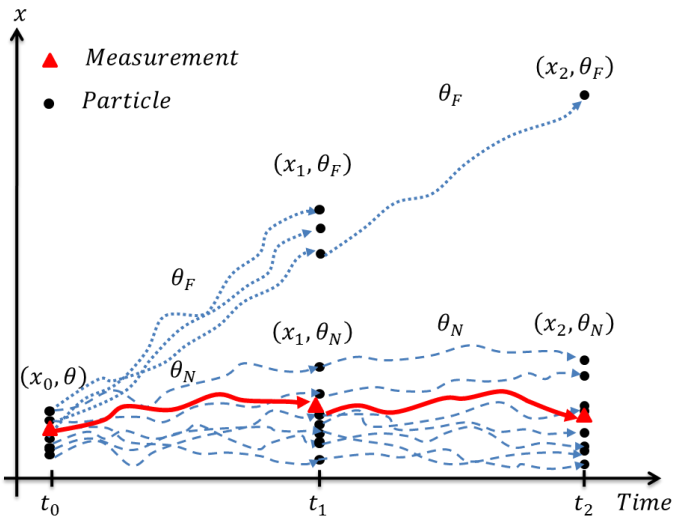

Fig. 3.5 Evolution of a system as long as measurements support the normal model.

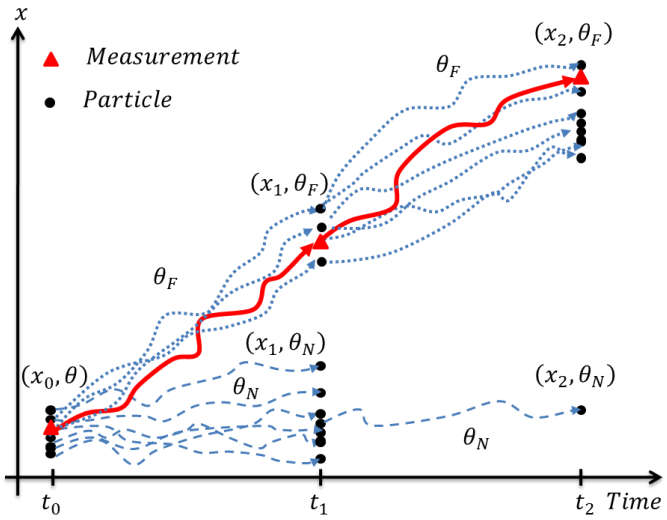

Fig. 3.6 Evolution of the system and correlated swap in the model parameter, due to measurement supporting the fault model.

In this framework, the probability associated to each operational model can be estimated at every time step by marginalizing the updated particle distribution:

$$\mu_k^i = p(\theta_k = m_i | \, \boldsymbol{y}_k) = \int p(\boldsymbol{x}_k \, , \theta_k | \, \boldsymbol{y}_k \,) \, d\boldsymbol{x}_k \tag{3.6}$$

From the practical point of view, this is equivalent to sum the updated probability masses of the particles simulated according to model m_i. On this basis, the probability of the system being in safe state is given by:

$$\mu_k^{safe} = p\big(\theta_k \in M_{safe} | \, \boldsymbol{y}_k\big) = \sum_{i=1}^{N} p\big(\theta_k = m_{n_i} | \boldsymbol{y}_k\big) \tag{3.7}$$

where $M_{safe} = \{m_{n1}, \dots \, , m_{n_N}\}$ is the set of all the normal active models. Fault detection can be based on the comparison of μ_k^{safe} with a proper threshold value μ_T (e.g., μ_T=0.05). That is, if $\mu_k^{safe} < \mu_T$, then it is reasonable to conclude that the system is in fault state.

With regards to fault isolation, the Maximum A Posteriori (MAP) criterion can be used to such aim [46]. In details, the model, say *D*, corresponding to the maximum value of μ_k^i is selected among all the possible models:

$$\mu_k^D = \max_{i=1,\dots,M} \mu_k^i \tag{3.8}$$

If model *D* is different from that currently used to describe the system evolution, and μ_k^D is considerably larger than the values μ_k^i associated to all the other

models, then a change in the system state is diagnosed. In this respect, to make more robust decisions and reduce the number of false alarms, one can require that this criterion is fulfilled for a number of consecutive time steps.

Finally notice that for the sake of generality, in the model considered in (3.3) the stochastic noise ω_{k,θ_k} depends not only on time, but also on the value of θ_k, i.e., on the operating model; this allows giving due account to the different variability of the alternative models. For example, if the amount of information about the normal system functioning is larger than that about a failure model, then the corresponding noise ω_{θ_i}, $\theta_i \in M_{failure} = \{m_{f1}, \dots, m_{f_F}\}$ is expected to have higher variability than ω_{θ_j}, $\theta_j \in M_{safe} = \{m_{n1}, \dots, m_{n_N}\}$.

3.4 CASE STUDY: Crack Degradation Process

As mentioned in Section 3.1, the case study considered in this work deals with the crack growth degradation process. The FDI performance of the method that relies on the augmented state (which is here labeled as IMM, according to the terminology used in [46]) is evaluated in two different settings:

1) There are only two models available, one for normal conditions and the other for degradation; hence, detection and diagnosis coincide. This is the same setting of other works of the literature (e.g., [39], [42]). Then, the performance of the IMM method is compared with those of the LLR-based method proposed in [12] (which is here referred to as Multiple Swarms (MS)) and of an intuitive, statistical approach.
2) A third degradation model is considered, in order to evaluate the diagnostic capability of the proposed approach in selecting the right model to describe the current evolution behavior.

3.4.1 Two-Model Setting: Fault Detection

3.4.1.1 Model Description

The crack growth evolution is here described as a two phase process:

1) crack incubation, which is modeled by a constant null value, since crack is too small to be measured:

$$m_n : x_k = 0 \tag{3.9}$$

2) crack propagation, which is modeled by the Paris-Erdogan model [40]:

$$m_f : x_k = x_{k-1} + C \cdot e^{\omega_k}\left(\beta \cdot \sqrt{x_{k-1}}\right)^n \tag{3.10}$$

where $\omega_k \sim N(0,\ 1)$ describes the uncertainty in the growth speed; $C = 0.005$ and $n = 1.3$ are parameters related to the component material, and $\beta = 1$ is an experimentally determined constant related to the characteristics of the load and the position of the crack. The values of these parameters are derived from [11], whereas the discretized time unit is here assumed to be expressed in arbitrary units of time.

The measurement model is:

$$y_k = \begin{matrix} v_k & , x_k \le mc \\ x_k + v_k & , x_k > mc \end{matrix} \tag{3.11}$$

where $v_k \sim N(0,\ 0.5)$ is an additive Gaussian measurement error. The measurement instrument is assumed to have a resolution $mc = 0.4$, which means that it is not capable of observing cracks with length $x_k \le mc$.

To conclude, Fig. 3.7 shows a possible crack evolution and the associated measures.

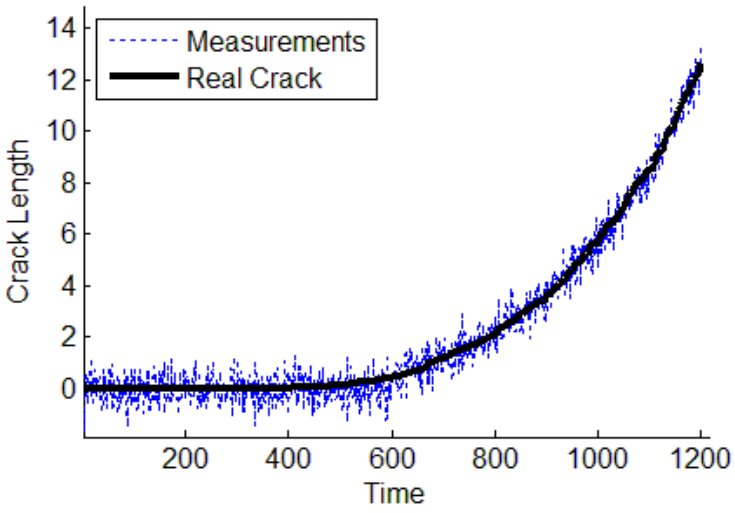

Fig. 3.7 Crack growth simulation of a crack started at $t_k = 400$h.

3.4.1.2 Interacting Multiple Model (IMM)

The transition probability matrix for the model parameter θ_k has been chosen as:

$$A_{trans} = \begin{bmatrix} 0.99 & 0.01 \\ 0.01 & 0.99 \end{bmatrix} \tag{3.12}$$

where the probabilities of particles changing the reference model are set, at a first attempt, to very small values, i.e., $A_{12} = A_{21} = 0.01$. This is justified by the following considerations:

a) with regards to A_{12}, the larger its value the larger the expected numbers of particles that start evolving according to the fault model. For example, if the number of particles is set to $N_{S_{IMM}} = 100$, then on average at every time step a particle of the swarm is forced to swap model. This entails that when a measure is acquired from a safe system, the particles with augmented variable set to θ_F are unlikely to be re-sampled, and the swarm continues evolving in the correct way. On the contrary, if the probability A_{12} were set to a larger value, e.g., 0.2, there would be 20 particles evolving according to the fault model. This means that the probability of having a particle re-sampled from this set

becomes large, especially in the presence of an outlier measurement. Hence, large values of A_{12} make the filter too much sensitive to the measurement noise, with the consequent increment in the probability of having false alarms.

b) With regards to A_{21}, it should be borne in mind that the speed of growth of the modeled crack, and thus of the particles evolving according to such model, is small. Furthermore, when the particles that are correctly associated to the variable $\theta_{k-1} = \theta_F$ are forced to change the prediction model (i.e., $\theta_k = \theta_N$), their crack lengths are reset to 0; thus, they need a long time to re-catch the real crack length. This entails that if the transitions $\theta_F \rightarrow \theta_N$ occur too much frequently, then the distribution of the particles turns out to be non-conservatively biased, with the consequent delay in crack detection. Typically, the smaller the speed of growth, the smaller should be A_{21}, as it is confirmed by the analysis below.

Fig. 3.8 shows the good filtering capability of the method, which emerges from the closeness of the filtered and simulated crack growth behaviors.

Notice also that in the present case study there are only 2 models available; then, fault detection coincides with diagnostics, and the marginalized distribution in Eq. (3.6) is split only between two discrete states. Hence, the alarm threshold can be set at a large value (e.g., $\mu_T = 0.985$) to guarantee a low probability of false alarm and a prompt detection. Fig. 3.9 shows an example of how the probability of being in a fault model has a steep increment and crosses the alarm threshold μ_T (dashed horizontal line) a few time steps after the time instant when the real crack has reached the mc threshold (dashed vertical line). In this respect, notice that as mentioned above, when the crack length is smaller than mc, it cannot be detected (Eq. (3.11)). Then, the optimal time $T_{optimal\ detection}$ to detect the crack is necessarily larger than the time instant at which the second phase of the crack growth process starts (bold continuous vertical line).

Notice also that the spike highlighted in Fig. 3.9 is due to an outlier measure, which could be considered as an observation acquired from a system with no crack. Nevertheless, the method shows its robustness, being the spike not capable to force a change in the model identification.

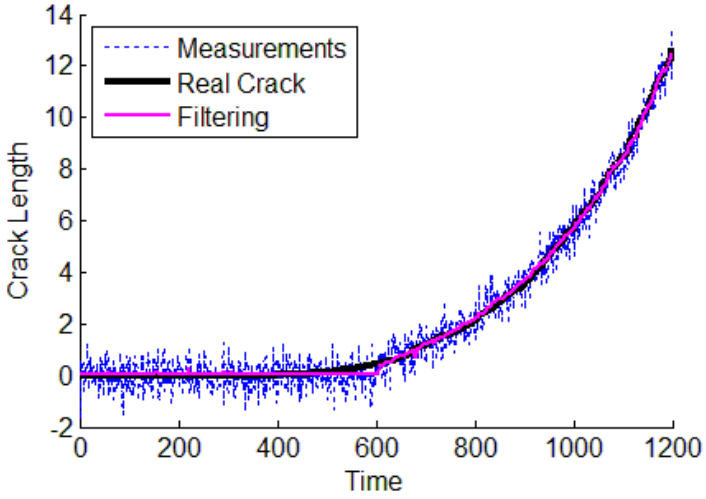

Fig. 3.8 Filtering crack's length via IMM method

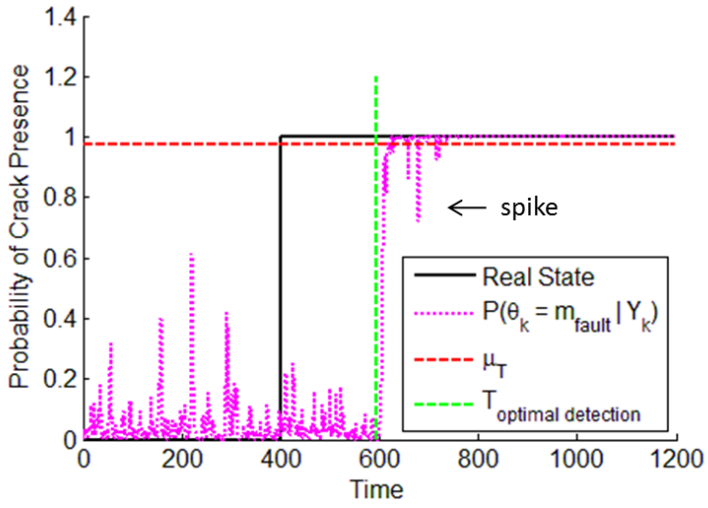

Fig. 3.9 Marginal posterior probability associated to fault model

3.4.1.3 Multiple Swarms (MS).

In this paragraph, the method proposed [12] is applied to the considered the two-model case study. The number of particles for each swarm is set to $N_s = 25$.

This guarantees that each swarm provides a robust statistics in support of the LLR test. The observation time window is set to $w = 100$, which is large enough to take into account the slow initial speed of growth. The minimum number of successive swarms that must identify abnormal conditions to detect a fault, is set to $n = 5$. This avoids possible false alarms induced by measurement outlier values.

Fig. 3.10 shows an example of crack evolution, with the filtered state estimated by the n out of w swarms that give the detection alarm. There is a very good matching between the real crack evolution and the mean value of the new swarms within the window $[\sim 560, \sim 660]$ units of time. In particular, according to the MS approach, the extent of such matching between the observations and the particle distribution is evaluated by a function $g(LLR)$ (details about this function can be found in [12] and[31]). Roughly speaking the higher its value, the larger the likelihood that the observations come from the abnormal model.

Fig. 3.11 reports the evolution of function g corresponding to the trial in Fig. 3.10. Notice that there is a sharp increment in $g(LLR)$ when the 5 swarms start evolving very close to the real crack.

The detection alarm is given when $g(LLR)$ crosses the threshold value λ, which is here set to 8. In this respect, to avoid false alarms λ must be such that when system evolves according to a normal model, possible consecutive measures larger than mc, which entail large values of $g(LLR)$, do not cause a change in the model. On the other side, setting λ to very large values leads to a delay in detection. Thus, $\lambda = 8$ is a compromise value between these two conflicting needs.

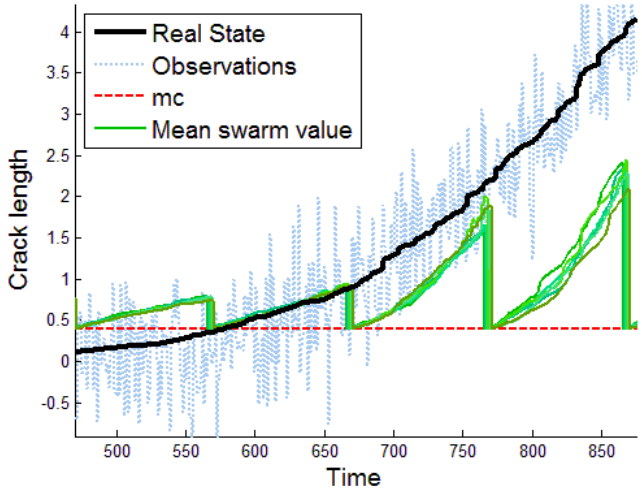

Fig. 3.10 Filtering crack length performed by the 5 swarms of particles giving alarm.

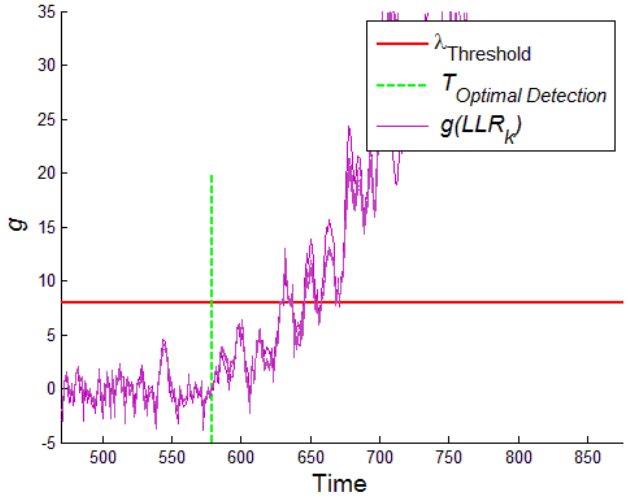

Fig. 3.11 Function of the LLR used to set the alarm conditions

3.4.1.4 Sequential Statistic Test (ST)

The detection methods discussed above are compared with an intuitive approach based on the statistical hypothesis test technique. In details, the test performed is a trivial Z-test for mean with known standard deviation, since the standard deviation of $\nu_k \sim N(0,\ 0.5)$ is assumed to be known. The null hypothesis H_0 is that the mean value of the measures is μ_y =0, whereas the

alternative hypothesis H_1 is that $\mu_y \geq 0$. This entails that H_0 is refused in favor of H_1 when there is the evidence of the crack presence.

To increase the robustness of the method, the alarm is given when H_0 is refused for an established number $seq_{ST} = 4$ of consecutive observations. Thus, if the I type error of each independent test is set to $\alpha_I = 0.1$, the null hypothesis is refused according to a I type error $\alpha_{ST} = {\alpha_I}^{seq_{ST}} = 10^{-4}$. In this respect, notice that if H_0 is true, then the observations are independent and identically distributed random variable.

3.4.1.5 Performance Indicators

To assess the performance of the different approaches, 100 cracks have been simulated, and used for evaluating the following three performance indicators:

- *Detection Time Delay* [51], i.e., $DTD = T_{detection} - T_{optimal\ detection}$, where $T_{optimal\ detection} = \min_k\{\, k : x_k > mc \,\}$. This is an indicator of the promptness of the method in detecting the change in the model.
- *Crack On Noise*, i.e., $CON = \frac{x_{T_{detection}}}{\sigma_v}$ which gives an information about length of the crack upon detection, compared to the amplitude of the measure uncertainty. Small values of this indicator relate to an accurate detection.
- *False Alarms*, i.e., the number of alarms given without that a crack has occurred. It is a wide spread index for the robustness of the method.

Notice that false alarms are of primary importance in condition monitoring, being the unnecessary stops of a plant for maintenance operation generally highly expensive. Thus, the 'work points' of the parameters of the considered detection techniques have been set such that the number of false alarms is around the acceptability level of 5%. This is supposed to be the best initial setting to allow a comparison between the three method.

Table 3.1 reports the average values of the three performance indicators, corresponding to the application of the three considered techniques to the 100 simulated crack growth trials. From this table, it emerges that the two filtering

methods IMM and MS have better performances than ST, being the mean values of the corresponding indicators smaller than those of ST. Moreover, although the performance in detection of IMM seems not much better than the performance of MS (2 unit of time, only), it must be kept in mind that IMM has a lower computational cost than MS, since it needs to run $N_{S_{IMM}} = 100$ particles instead of $N_{S_{MSTotal}} = N_{S_{MS}} \cdot w = 25 \cdot 100 = 2500$ particles simultaneously simulated in the MS approach. Table 3.2 reports the computational time necessary for filtering the evolution of one simulated crack growth in seconds.

Notice also that the IMM commits less False Alarms than MS, see Table 3.1.

	ST	**IMM**	**MS**
DTD	44.3	19.8	22.1
CON	1.295	1.001	1.025
False Alarms	6%	3%	6%

Table 3.1 Detection Time Delay, Crack On Noise and Percentage of false alarms evaluated on a sample of 100 simulated cracks, for the three methods.

	IMM	**MS**
Computational Time (sec)	1.7	32

Table 3.2 Computational time for filtering a crack growth according to the two PF method analyzed.

Finally, sensitivity analyses have been performed to evaluate the dependencies of the performance from the transition probabilities and the variability of the measurement noise.

In details, the sensitivity of the methods to the transition probability matrix has been investigated by varying both the extra-diagonal elements of the matrix A_{trans} within the set $\{0.005, 0.01, 0.05, 0.1\}$, and correspondingly the values on its diagonal. Table 3.3 shows that the larger the probability of transition, the poorer the DTD and CON indicators. These results come from the fact that if transitions from a model to another are too frequent, then crack length is reset to null too often, thus preventing the particles from swapping to the correct

model. This suggest that when setting the transition matrix, both probability of occurrence and speed of growth of the crack must be taken into account. On the other side, if the probability of transition is very small, i.e., A_{12}= 0.005, the method of augmenting the state space becomes useless, as on average we have 1 out of 100 particles changing the reference model every two steps. This consideration explains the worsening of the performance corresponding to A_{12}= 0.005.

A_{12}	**0.005**	**0.01**	**0.05**	**0.1**
DTD	20.1	18.6	25.1	38.6
CON	1.017	0.9963	1.053	1.237
False Alarms	0%	1%	0%	0%

Table 3.3 Detection Time Delay, Crack On Noise and Percentage of false alarms evaluated on a sample of 100 simulated cracks, for the three methods.

A sensitivity analysis has been also carried out for the uncertainty in the measurement error. The three considered performance indicators have been evaluated according to different values of the standard deviation of the measurement noise $\sigma_v \in \left\{\frac{1}{8}, \frac{1}{4}, \frac{1}{2}, 1, 2, 4, 8\right\} \cdot \sigma_{v\,rif}$. This entails that σ_v takes values of different magnitude with respect to the measurement resolution mc: when $\sigma_v = 8 \cdot \sigma_{v\,rif} = 4$, then the precision in the measurement system is very low, whereas it is really high when $\sigma_v = \frac{1}{8} \cdot \sigma_{v\,rif} = \frac{1}{16}$. In Table 3.4 and Table 3.5 the 90th percentile of every performance indicator is considered as a synthetic and conservative indicator of the promptness of the detection of the three methods. In this respect, other parameters to summarize the distribution such as the mean, the median, etc., would put emphasis on the performance of the detection methods in the best cases, whereas the 90th encompasses also the performance of the methods in the worst cases.

From Table 3.4, it emerges that the DTD values of the three methods are similar for small values of σ_v, whereas the IMM method is by far the most accurate when σ_v is comparable with or higher than the measurement resolution mc.

That is, when the measurement error is very small, all the methods are capable of distinguishing the fault condition from the normal behavior. This result is also confirmed by Table 3.5, even though apparently it seems to confirm the opposite conclusion. In this respect, is must be considered that the larger CON values in correspondence of small values of σ_v are due to the resolution of the measurement system which is fixed to mc =0.4. That is, as long as the real crack is shorter than mc, the measurement system cannot observe any variation, thus no detection can occur until it is long at least mc. Hence also the optimal value of CON (the crack is detected exactly when it reaches mc) takes large value. For example, the optimal CON according to σ_v=0.0675 is $\frac{mc}{\sigma_v} = \frac{0.4}{0.0675} = 5.93$.

Notice that, the decreasing performances of the method proposed in [12] are related to its need of a larger window to catch the difference between the two models. This is confirmed by the ascending values of the 90th percentile of MS, $q_{0.9}(CON)$, for large value of σ_v. However, even if w is set to its best value (i.e., w=300), its DTD is still worse than that of IMM (see Fig. 3.12), and also with higher computational costs (e.g. according to Table 3.2, the computational time is three times longer, ~95 sec / crack). Finally, Table 3.6 reports the percentage of false alarms for the different values of σ_v. This performance indicator is constant for ST; this is due to the fact that the value of the standard deviation enters directly the statistical tests, which have the same I type error value α_{ST}. With respect to both the PF-based methods, the false alarm percentage is not-null only if the standard deviation takes intermediate values, i.e., when σ_v takes a value similar to mc. This is due the fact that the smaller σ_v, the more similar are the observations to the real crack length. Thus the reconstruction provide by the PF is more accurate. On the other side, the larger σ_v, the larger the probability of acquiring observations having small values, i.e., observations which can avoid particles to grow or which can change the model parameter resetting the length of the crack associated (only for the IMM). Thus both the methods become more conservative.

σ_v	0.0675	0.125	0.25	0.5	1	2	4
ST $q_{0.9}(DTD)$	4	6	19,2	73,2	155	257	387,3
IMM $q_{0.9}(DTD)$	3	5	12,6	29	71,6	151,6	248
MS $q_{0.9}(DTD)$	1	3	10	36	123	275	569,5

Table 3.4 90th percentiles of the DTD performance indicator for ST, IMM and MS, and for increasing values of the standard deviation of the measurement noise.

σ_v	0.0675	0.125	0.25	0.5	1	2	4
ST $q_{0.9}(CON)$	7,02	3,55	2,01	1,67	1,49	1,42	1,35
IMM $q_{0.9}(CON)$	6,88	3,54	1,88	1,11	0,83	0,74	0,68
MS $q_{0.9}(CON)$	6,76	3,46	1,85	1,21	1,24	1,59	2,74

Table 3.5 90th percentiles of the CON performance indicator for ST, IMM and MS, and for increasing values of the standard deviation of the measurement noise.

σ_v	0.0675	0.125	0.25	0.5	1	2	4
ST False Alarms	6	6	6	6	6	6	6
IMM False Alarms	0	0	1	3	3	1	0
MS False Alarms	0	4	10	6	0	0	0

Table 3.6 Percentage of false alarms evaluated for different values of the standard deviation of the measurement noise.

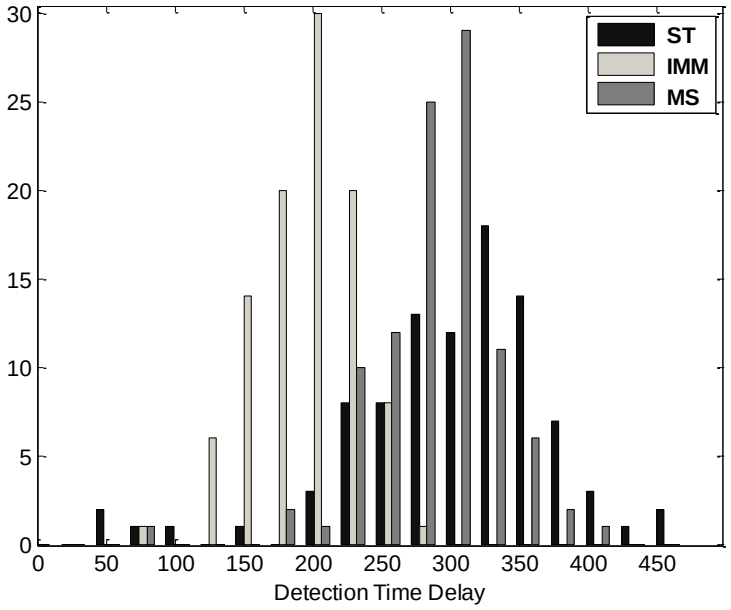

Fig. 3.12 DTD using $w = 300$ for the MS method.

3.4.2 **Three-Model Setting: Fault Detection and Diagnostic**

The objective of this case study is to evaluate the diagnostic capability of the IMM PF, i.e., the quickness and accuracy in identifying the model that better describes the evolution of the system. In this regard, the three-phases model for crack propagation introduced in Section 2 has been considered. The models available are:

1) incubation, which is described by a constant process, since crack is too small to be measured:

$$m_n : x_k = 0 \tag{3.13}$$

2) crack initiation, which is modeled by a linear process:

$$m_{f1} : x_k = x_{k-1} + a \cdot e^{\omega_k^1} \tag{3.14}$$

where $a = 0.003$ is the speed of growth parameter, and $\omega_k^1 \sim N(-0.625,\ 1.5)$ modes the uncertainty in the speed;

3) crack rapid-propagation, which is again described by the Paris-Erdogan model:

$$m_{f2}: x_k = x_{k-1} + C \cdot e^{\omega_k^2} \left(\beta \cdot \sqrt{x_{k-1}}\right)^n \quad \textbf{(3.15)}$$

where the parameter values are the same of the two model system.

The measurement system is that in Eq. **(3.11)**, with the same parameter values. Notice that the distribution of the noise in the initiating phase is different from that in the rapid-propagation phase. This gives due account to the fact that the evolution of an incipient crack is highly influenced by exogenous factors, and hardly measurable due to its small length. Hence, its uncertainty is expected to be larger.

Fig. 3.13 reports the simulation of possible crack evolutions, whereas a possible measure of a crack degradation process is represented in Fig. 3.14. All the simulated crack growth processes start at $T_{Crack} = 400$ units of time, and follow the initiating linear model in Eq. **(3.14)** up to $T_{PE} = 800$ units of time, when they switch to the Paris-Erdogan model in Eq. **(3.15)**. In this respect, notice that the performance indicators are related to the identification delay time; then, the choice of setting a fixed swap time does not affect the generality of the results.

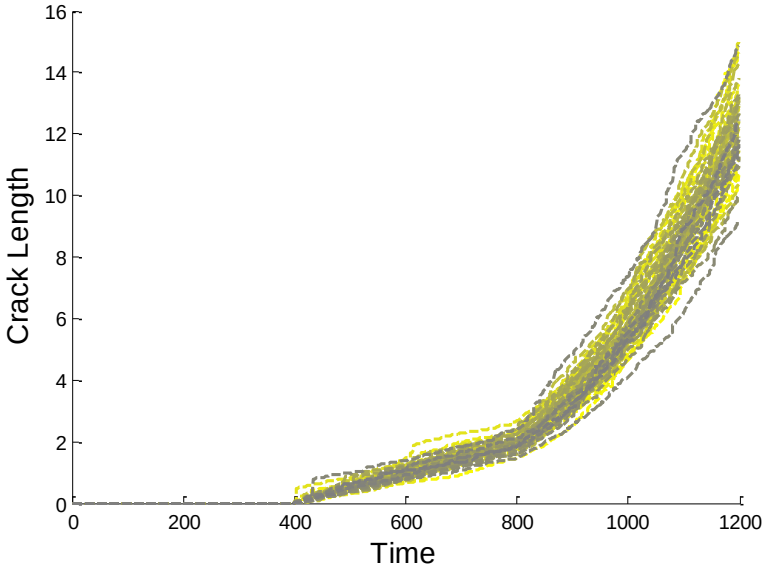

Fig. 3.13 Simulation of 30 cracks with the same starting time step $T_{crack} = 400$ and same swicth time step to P-E model $T_{PE} = 800$.

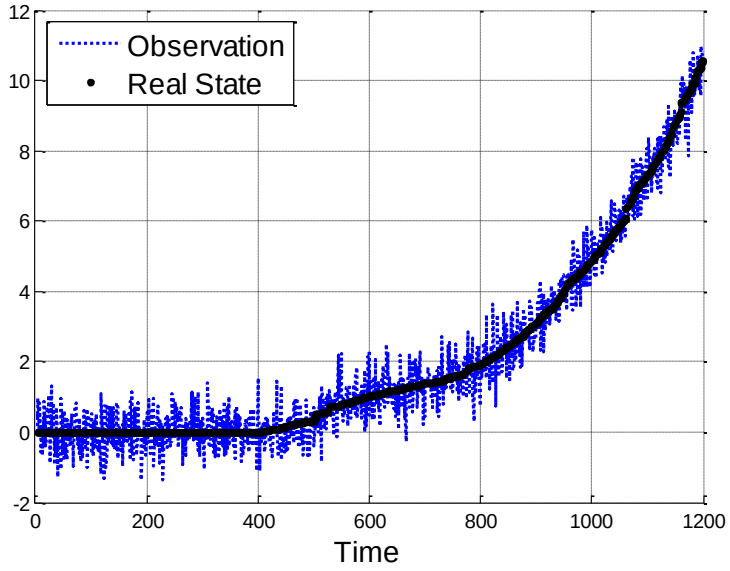

Fig. 3.14 Trajectory of a simulated crack and a respectively possible measurement process (dot line).

Performances have been tested by simulating $N_{Crack} = 500$ crack growth processes, and evaluating the following performance indicators:

- Detection Time Delay (DTD), which is the time span between the start of the initiating phase and its detection.

- Transition Time Delay (TTD), which is the time span between the start of the rapid-propagation phase and its detection.
- Percentage of False alarms, which can concern both the two transitions.

On the basis of considerations similar to those of the previous cases study, the transition probability matrix is set to:

$$A_{trans} = \begin{bmatrix} 0.98 & 0.015 & 0.005 \\ 0.01 & 0.98 & 0.01 \\ 0.005 & 0.005 & 0.99 \end{bmatrix} \quad \textbf{(3.16)}$$

The number of particles is set to $N_S = 100$ as in the previous case study, and the detection threshold is set to $\mu_T = 0.8$, with a number $seq_{detection} = 5$ of consecutive detections required to give the detection alarm.

Fig. 3.15 shows that the IMM is able to detect the changes in the operational models on the basis of the marginal posterior probability in Eqs. **(3.6)** and **(3.8)**, with good filtering performances, as confirmed by Fig. 3.16. Indeed, in the first phase (i.e., $k < T_{crack} = 400$) the marginal probability μ_k^1 associated to the incubation model takes by far the highest value; in the second phase (i.e., $T_{crack} < k < T_{trans} = 800$) the probability μ_k^2 of the initiating model takes by far the highest value, whereas in the last phase the value μ_k^3 associated to the rapid-propagation model takes the highest value.

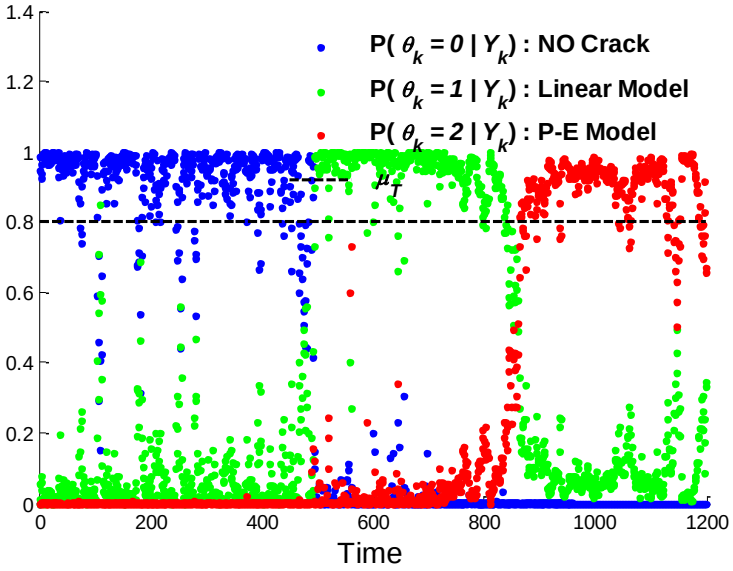

Fig. 3.15 Marginal posterior probability for every operating models.

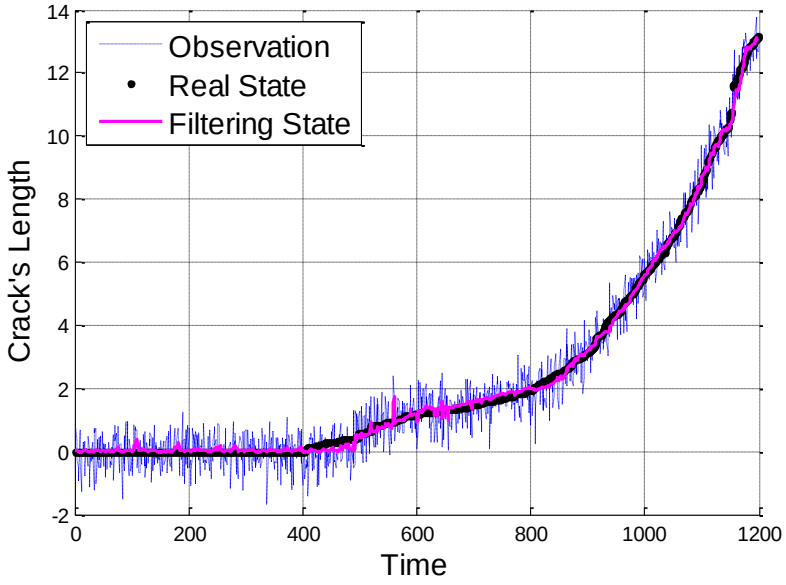

Fig. 3.16 IMM filtering of the real length of the crack.

Notice that the identification of the transition between incubation and initiating model (i.e., $m_n \rightarrow m_{f1}$) is more accurate than that between the initiating and the rapid-propagation models (i.e., $m_{f1} \rightarrow m_{f2}$), as it emerges from the large

time window in which there is high uncertainty in the variable *D* to be associated to μ_k^D (i.e. the high overlapping in the time span $[\sim 800, \sim 900]$ in Fig. 3.16) . In this respect, Fig. 3.17 and Fig. 3.18 show that the distribution of the DTD is centered on a smaller value and presents a sharper shape than that of the distribution of the TTD. This is due to the smooth transition between the propagation models in Eqs. **(3.14)** and **(3.15)**, as confirmed by the percentage of false alarms reported in Table 3.7, which is smaller in the first transition. Different choices of μ_T and $seq_{detection}$ entail different performances. Intuitively, small values of $seq_{detection}$ and μ_T make the method sensitive to possible outliers related to measurement noise, as it is confirmed by the high percentage of false alarms, see Fig. 3.19. On the other side, large values of $seq_{detection}$ and μ_T make the method more conservative, as it is confirmed by the increased delay in DTD and TTD.

Finally, Table 3.8 and Table 3.9 report the 90th percentile of the DDT and TTD for increasing values of $seq_{detection}$ and μ_T, respectively. As expected, the percentile take value in ascending order according to both increasing value of $seq_{detection}$ and μ_T

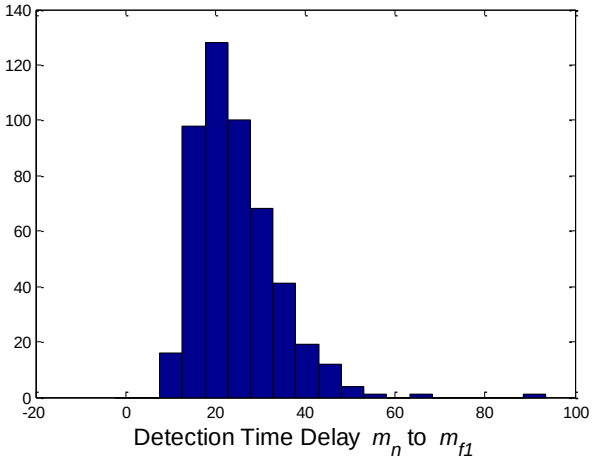

Fig. 3.17 Histogram of the DTD from the incubation model to the initiating model.

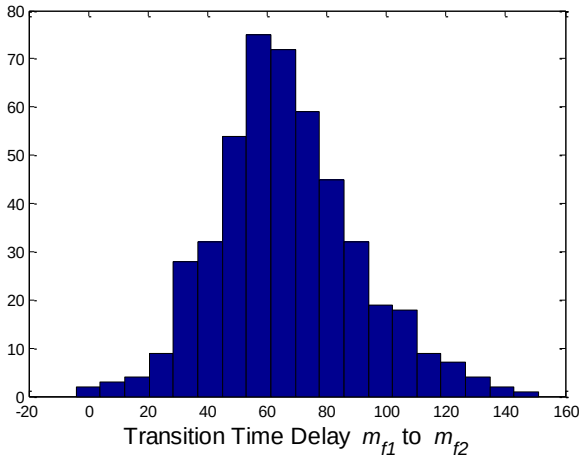

Fig. 3.18 Histogram of the TTD from the initiating model to the P-E model.

Transition	$\boldsymbol{m_n \rightarrow m_{f1}}$	$\boldsymbol{m_{f1} \rightarrow m_{f2}}$
False Alarms	2.2%	5%

Table 3.7 Percentage of false alarms evaluated on 500 simulated cracks.

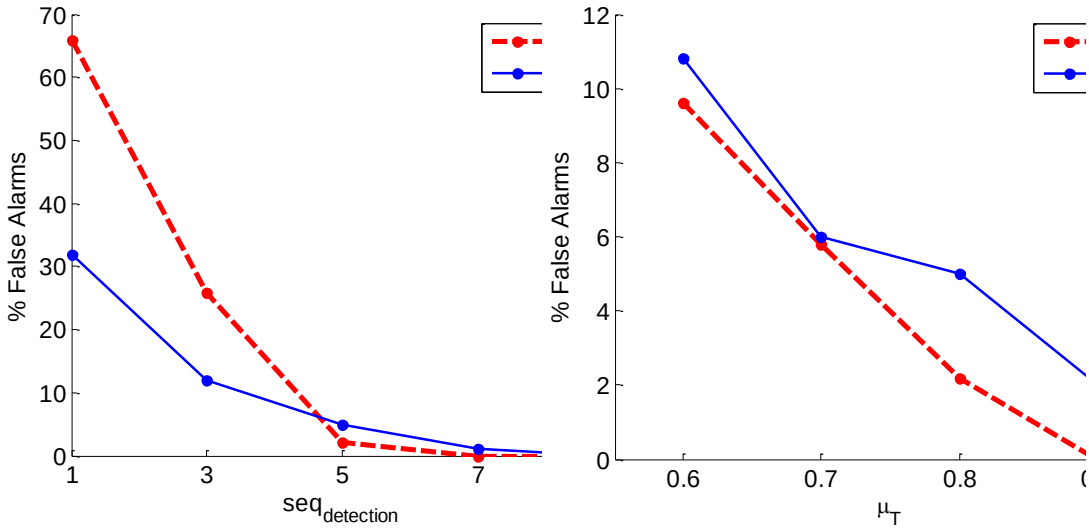

Fig. 3.19 percentage of false alarms: Left column sensitivity to $seq_{detection}$; right column sensitivity to μ_T.

$seq_{detection}$	1	3	5	7	9
$q_{0.9}(DTD)$	17	23	36	67	142,5
$q_{0.9}(TTD)$	75,8	81	99	134,1	187

Table 3.8 90th percentile of DTD and TTD for ascending values of consecutive detection.

μ_T	0.6	0.7	0.8	0.9
$q_{0.9}(DTD)$	30	31	36	50
$q_{0.9}(TTD)$	78	86,5	99	146

Table 3.9 90th percentile of DTD and TTD for ascending values of the detection threshold.

3.5 Conclusion

This chapter has investigated the potential of a PF approach based on an augmented state vector for fault detection and isolation in nonlinear multi-

model smooth degradation processes. By way of a case study concerning the crack growth degradation process, it has been shown that such approach, referred to as IMM, is capable of performing an accurate and prompt detection of the crack occurrence, and provides also a robust estimation of the real length of the crack. Furthermore, the diagnostic capability of this method has been confirmed even when the degradation process is modeled evolving among three phases, with smooth transitions from one phase to another.

The performance of the IMM method have been compared to those of an already available PF technique of the literature, and of a statistical sequential test method by way of a two-phase crack degradation process. It has emerged that the FDI performance of the IMM techniques is better than those of the other two methods, regarding prompt detection and computational cost.. Moreover, the introduction of the augmented state which explicitly indicates the process phase, makes the FDI problem much more easily comprehensible. Indeed, the information provided by the method is the probability that the monitored component is in a specific degradation phase,.

4

Conclusions

In this work, fault detection of industrial components has been considered. Two novel contributes which aim at an early and accurate identification of the incipient abnormal condition of the component behavior, have been proposed. Respectively the former regarding data-driven methods, the latter model-based methods. With respect to data-driven methods, this work has focused on the AutoAssociative Kernel Regression (AAKR). In order to obtain more robust signal reconstructions of the expected values of the monitored signals in normal conditions, a modification of the traditional AAKR method has been proposed. The modification is based on a different procedure for the computation of the similarity between the present and the historical measurements. In particular, before the computation of the Kernel between the two vectors, which is performed as in the traditional AAKR method according to a Gaussian RBF function, the data are projected into a new signal space defined by using a penalization vector which reduces the contribution of signals affected by malfunctioning. The procedure is based on the hypothesis that the probability of occurrence of a fault causing variations on a large number of signals is lower than that of one causing variations on a small number of signals.

The modified AAKR method has been applied to a real case study concerning the monitoring of 6 highly correlated signals in an industrial plant for energy production. The possibility of detecting sensor faults has been investigated. The obtained results have shown that the reconstructions provided by the modified AAKR are more robust than those obtained by using the traditional AAKR. This causes a reduction in the time necessary to detect abnormal conditions and in a more accurate identification of the signals actually affected by the abnormal conditions.

On the other side, with respect to model-based methods, this work has focused on a Particle Filtering PF approach based on an augmented state vector where the augmented state represents the possible behavior of the component. At the best of the author's knowledge, this is the first time, that it has been applied for detection and diagnostic where more than two models are available, the noise in the model is non-Gaussian and the degradation process is smoothly evolving. By way of a case study concerning the crack growth degradation process, it has been shown that such approach, referred to as IMM, is capable of performing an accurate and prompt detection of the crack occurrence, and provides also a robust estimation of the real length of the crack. The performances of the IMM method have been compared to those of an already available PF technique of the literature, and of a statistical sequential test method by way of a two-phase crack degradation process. It has emerged that the FDI performances of the IMM techniques are better than those of the other two methods. Furthermore, the method has been capable of diagnosing the correct phase degradation even when the degradation process is modeled as evolving among three phases, with smooth transitions from one phase to another. Finally, the introduction of the augmented state which explicitly indicates the process phase, makes the results of FDI problem easily comprehensible since the information provided by the method is the probability of being in a specific degradation phase.

To conclude, according to the data-driven method, future works will be devoted to the demonstration that the whole procedure proposed for the evaluation of

the weights, i.e. the pre-processing step and the application of a Gaussian kernel, is itself a kernel function. The application of the method to additional real case studies of degradation of components is also foreseen.

On the other side the diagnostic ability of the model-based method provides a good framework for developing some decision-making criteria. In this respect, future works will focus on the introduction in the model of a risk function, which takes into account the costs associated to false alarms and to identification delays. This could give the opportunity of developing a risk-based FDI.

References

[1] Alrowaie F., R.B.Gopaluni n, K.E.Kwok, 2012, "*Fault detection and isolation in stochastic non-linear state-space models using particle filters*", Control Engineering Practice, vol. 20, 1016–1032.

[2] Arulampalam S., Maskell S., Gordon N., Clapp T., 2002, "*A tutorial on particle filters for on-line nonlinear/non-Gaussian Bayesian tracking*", IEEE Transaction on Signal Processing, vol. 50, No. 2, pp. 174-188.

[3] Baraldi P., Canesi R., Zio E., Seraoui R., Chevalier R., 2011, *"Genetic algorithm-based wrapper approach for grouping conditional monitoring signals of nuclear power plant system"*, Integrated computer-Aided engineering, vol. 18,pp. 221-234.

[4] Baraldi P., Di Maio F., Pappaglione L., Zio E. and Seraoui R., 2012, *"Condition Monitoring of Power Plant Components During Operational Transients"*,Journal of Risk and Reliability.

[5] Baraldi P., Gola G., Zio E., Roverso D., Hoffman M., 2011, *"A randomize model ensemble approach for reconstructing signals from faulty sensors"*, Expert systems with application, vol 38, No. 8.

[6] Baraldi P., Mangili F., Zio E., 2012, *"A Kalman filter-based ensemble approach with application to turbine creep prognostics"*, IEEE Transaction on Reliability, vol. 61, No. 4, pp. 966-977.

[7] Basseville M., 1988. "*Detecting Changes in Signals and System – A survey*", Automatica, vol. 24, No. 3, pp. 309-326.

[8] Bishop C., 1995, "*Neural Networks for Pattern Recognition*", Oxford University Press, NY, USA.

[9] Boursier J.M., Desjardins D. and Vaillant F., 1995, *"The Influence of the strain-rate on the stress corrosion cracking of alloy 600 in high temperature primary water"*, Corrosion Science, vol. 37, No. 3, pp. 493-508.

[10] Burges C. J.C., 1998, *"A Tutorial on Support Vector Machines for Pattern Recognition",* Data Mining and Knowledge Discovery, vol. 2., pp. 121-167

[11] Cadini F., Zio E., Avram D., 2009, "*Model-based Monte Carlo state estimation for condition-based component replacement*", Reliability Engineering and System Safety, vol. 94,pp. 752-758.

[12] Cadini F., Zio E., Giovanni Peloni, 2012, "*Particle Filtering for the Detection of Fault Onset Time in Hybrid Dynamic Systems With Autonomous Transitions*", IEEE Transaction on reliability, vol. 61, No. 1, pp. 130-139.

[13] Candy J.V., 2009, "*Bayesian Signal Processing: Classical, Modern and Particle Filtering Methods*", IEEE and Wiley, New Jersey.

[14] Castanier B., C.Bérenguer and Grall A., 2003, *"A sequential condition-based repair/replacement policy with non-periodic inspections for a system subject to continuous wear"*, Applied Stochastic Models in Business and Industry, vol. 19, No 4, pp. 327-347.

[15] Chevalier R., Provost D., and Seraoui R., 2009, *"Assessment of Statistical and Classification Models For Monitoring EDF's Assets"*,Sixth American Nuclear Society International Topical Meeting on Nuclear Plant Instrumentation.

[16] Di Maio, F.; Baraldi, P.; Zio, E.; Seraoui, R., 2013, *"Fault Detection in Nuclear Power Plants Components by a Combination of Statistical Methods,"* Reliability, IEEE Transactions on, Accept, not published.

[17] Doucet A. N., Johansen A. M., 2008, "*A Tutorial on particle filtering and smoothing: Fifteen years later*".

[18] Doucet. A., N. De Freitas and N.J. Gordon, 2001, *"An introduction to Sequential Monte Carlo Methods"* in SMC in Practice, Springer-Verlag, New York.

[19] Dunia R., Qin S.J., Edgar T.F., McAvoy T.J., 1996, *"Identification of Faulty Sensors Using Principal Component Analysis"*, AlChE Journal, vol.42, No.10, pp. 2797-2811.

[20] Feller S., Todorov Y., Jaroszewski D., Chevalier R., 2013, *"Taming Anomaly Detection for Industrial Applications"*, AIP Conference Proceedings, vol. 1558, pp. 2257-2260

[21] Gordon, N. J., Salmond, D. J., and Smith, A. F. M., 1993, *"Novel approach to non-linear/non-Gaussian Bayesian state estimation"*, IEE Proceedings–F, 140, 107–113.

[22] Grall, A., Blain, C., Barros, A., Lefebvre, Y., F.Billy, 2007, *"Modeling of Stress Corrorsion Cracking with Periodic Inspection",* Proceeding of the 32nd ESReDA Seminar, Alghero, Italy Maintenance Modeling and Application, vol. 1, pp. 253-260.

[23] Guglielmi G., Parisini T., Rossi G., 1995, *"Fault Diagnosis And Neural Networks: A Power Plant Application"*, Control Engineering Practice, vol. 3, No. 5, pp. 601-620.

[24] Harkat M.F., Djelel S., Doghmane N., Benouaret M., 2007, *"Sensor Fault Detection, Isolation and Reconstruction Using Nonlinear Principal Component Analysis"*, International Journal of Automation and Computing, vol. 4, No. 2, pp. 149-155.

[25] Henk A., Blom P., Bar-shalom Y., 1988, "*The interacting multiple model algorithm for system with Markovian switching coefficients*", IEEE Transactions on Automatic Control, vol. 33, No. 8.

[26] Hines J. W., Garvey D., 2006, *"Development and Application of Fault Detectability Performance Metrics for Instrument Calibration Verification and Anomaly Detection"*, Journal of Pattern Recognition Research, vol. 1, pp. 2-15.

[27] Hines J. W., Garvey D., 2007, *"Process and Equipment Monitoring Methodologies Applied to Sensor Calibration Monitoring"*, Quality and Reliability Interantional, vol. 23, No. 1, pp. 123-135.

[28] Hsu C., Chang C., Lin C., 2003, *"A Practical Guide to Support Vector Classification",* Department of Computer Science and Information Engineering, National Taiwan University, Taipei.

[29] Jardine A., Lin D., Banjevic D., 2006, "*A review on machinery diagnostics and prognostics implementing condition based maintenance"*, Mechanical Systems and Signal Processing, vol. 20, No. 7, pp. 1483–1510.

[30] Julier, S. J. and Uhlmann, J. K., 1997, *"A new extension of the Kalman filter to nonlinear systems"*, SPIE Aerospace Symposium.

[31] Kadirkamanathan V., Li P., 2001, *"Particle Filtering based likelihood ration approach to fault diagnosis in nonlinear stochastic system"*, IEEE Transaction on Systems, Man and Cybernetics – part C: Application and Reviews, vol. 31, No. 3,pp. 337-343.

[32] Kadirkamanathan V., Li P., 2004, "*Fault detection and isolation in non-linear stochastic systems–A combined adaptive Monte Carlo filtering and likelihood ratio approach*", International Journal of Systems Science, vol. 77, No. 12, pp. 1101–1114.

[33] Kadirkamanathan V., Li P.,Jawardand M., Fabri S., 2002, "*Particle filtering-based fault detection in nonlinear stochastic systems"*, International Journal of Systems Science, vol. 33, No. 4, pp. 259–265.

[34] Liu J.S., Chen R., 1998, "*Sequential Monte Carlo method for dynamic system*", Journal of the America Statistic Association, vol. 93, No. 443.

[35] Liu W., Principe J., Haykin S., 2010, *"Kernel Adaptive Filtering: A Comprehensive Introduction*", John Wiley, Hoboken, New Jersey, USA.

[36] Mehra, M. Rago, C. and Seereeram, S., 1998, *"Autonomous failure detection, identification and fault-tolerant estimation with aerospace applications"*, in Proceedings of IEEE Aerospace Conference, Vol. 2, pp.133-138.

[37] Mehra, M., Seereeram, S., Bayard, D. and Hadaegh, F., 1995, *"Adaptive Kalman filtering, failure detection and identification for spacecraft attitude estimation"*, in Proceedings of the 4th IEEE Conference on Control Applications, pp.176-181.

[38] Nabeshima K., Suzudo T., Suzuki K., Turcan E., 1998, *"Real-time Nuclear Power Plant Monitoring with Neural Network"*, Journal of Nuclear Science and Technology,vol. 35, No. 2, pp. 93-100.

[39] Orchard M., Vachtsevanos G., 2009, *"A particle-filtering approach for on-line fault diagnosis and failure prognosis",* Transactions of the Institute of Measurement and Control, vol. 31,No. ¾, pp. 221–246.

[40] Paris P., Erdogan F., 1963, *"A Critical Analysis of Crack Propagation Laws"*, Journal of Basic Engineering, vol. 85, No. 4, pp. 528-533.

[41] Rasmussen C., Williams C., 2006, *"Gaussian Processes for Machine Learning*", MIT Press, Cambridge, MA, USA.

[42] Thrun S., Langford J., Verma V., 2001, *"Risk sensitive particle filters",* Advances in Neural Information Processing Systems, vol. 14.

[43] Venkatasubramanian V., R. Rengaswamy, K. Yin, S. N. Kavuri, 2003, "*A review of process fault detection and diagnosis Part I: Quantitative model-based methods*", Computers and Chemical Engineering, vol. 27, pp. 293-311.

[44] Venkatasubramanian V., R. Rengaswamy, S. N. Kavuri, 2003, "*A review of process fault detection and diagnosis Part II: Qualitative models and search strategies*", Computers and Chemical Engineering, vol. 27, pp. 313-326.

[45] Venkatasubramanian V., R. Rengaswamy, S. N. Kavuri, K. Yin, 2003, "*A review of process fault detection and diagnosis Part III: Process history based methods*", Computers and Chemical Engineering, vol. 27,pp. 327-346.

[46] Wang X., Syrmos V. L., 2008, "*Interacting Multiple Particle Filters For Fault Diagnosis of Non-linear Stochastic Systems*", American Control Conference, Seattle, USA.

[47] Willsky A.S. et al., 1980, "*Dynamic model-based techniques for the detection of incidents on freeways*", IEEE Trans. Automat. Contr., vol. AC-25.

[48] Worden K., Staszewski W., Hensman J., 2011, *"Natural computing for mechanical systems research: a tutorial overview"*, Mechanical Systems and Signal Processing, vol. 25, No. 1,pp. 4–111.

[49] Zhang B., Sconyers C., Byington C., Patrick R., Orchard M., Vachtsevanos G., 2008, *"Anomaly detection: a robust approach to detection of unanticipated faults"*, International conference on prognostics and health management.

[50] Zhang B., Sconyers C., Byington C., Patrick R., Orchard M., Vachtsevanos G., 2011, *"A probabilistic fault detection approach: application to bearing fault detection"*, IEEE transaction on industrial electronics, vol. 58, No. 5., 2011-2018.

[51] Zio E., 2013, *"Diagnostic and Prognostic of Engineering System: Methods and Techniques"*, IGI Global, pp. 333-356.

Appendix:

Particle Filtering

Particle Filtering (PF) has roots in the Bayesian framework and roughly speaking it consists in the approximation of the distribution of interest via a sequence of empirical distributions. To the best reader comprehension the appendix is structured as follow: section A.1 Nonlinear Bayesian Filtering presents the nonlinear bayesian filtering; section A.2 Monte Carlo Perfect Sampling reports monte carlo perfect sampling; in section A.3 Particle Filtering the Sequential Monte Carlo (SMC) method a.k.a. Particle Filtering is introduced; section A.4 Sequential Importance Resampling (SIR) present structure of the algorithm. An exhaustive dissertation could be found in [2], [13], [17], [18], [21].

A.1 Nonlinear Bayesian Filtering

Nonlinear filtering is defined as the process of estimating the state vector governed by a nonlinear, non-Gaussian state-space model (A.1), using noisy observation (A.2). Although a continuous-time estimation procedure can be performed, usually a discrete-time implementation is used since the streaming measurements data is sent and received through digital devices in most of the application regarding fault detection and diagnostic.

$$\boldsymbol{x}_k = \boldsymbol{f}_k(\boldsymbol{x}_{k-1}, \boldsymbol{\omega}_{k-1}) \tag{A.1}$$

$$\boldsymbol{y}_k = \boldsymbol{g}_k(\boldsymbol{x}_k, \boldsymbol{v}_k) \tag{A.2}$$

Within a Bayesian general formulation, filtering consists in the estimation of the posterior probability density function (pdf) of the current state $\boldsymbol{x_k}$, based on the set of received measurements. Since filtering is perform every time that a new observation arrived, to avoid an increasing computational cost and memory storage, a recursive strategy is pursued. Mathematically, let $\{\boldsymbol{x}_k\}_{k\geq 1}$ be an unobserved process described by a Markov Chain on χ described by its initial distribution $p(\boldsymbol{x}_0)$ and the transition probability $p(\boldsymbol{x}_k \mid \boldsymbol{x}_{k-1})$. $p(\boldsymbol{x}_k \mid \boldsymbol{x}_{k-1})$ is defined by the state equation (A.1) and the sequence of independent random variables $\{\boldsymbol{\omega}_k\}_{k\geq 1}$. Noisy measurements $\{\boldsymbol{y}_k\}_{k\geq 1}$ are observable and assumed to be conditionally independents given the process $\{\boldsymbol{x}_k\}_{k\geq 1}$, equation (A.2) defines the pdf $p(\boldsymbol{y}_k \mid \boldsymbol{x}_k)$ where $\{\boldsymbol{v}_k\}_{k\geq 1}$ is a sequence of independent random variable. Let $\boldsymbol{x}_{0:k} := \{\boldsymbol{x}_0, \dots, \boldsymbol{x}_k\}$ and $\boldsymbol{y}_{0:k} := \{\boldsymbol{y}_0, \dots, \boldsymbol{y}_k\}$ be, respectively, the state and the measurements up to time t_k; typical quantity of interest are: the *posterior distribution* $p(\boldsymbol{x}_{0:k} \mid \boldsymbol{y}_{0:k})$, the marginal distribution $p(\boldsymbol{x}_k \mid \boldsymbol{y}_{0:k})$ (a.k.a. *filtering distribution*) and the expectations:

$$I(h) = E_{p(\boldsymbol{x}_{0:k} \mid \boldsymbol{y}_{0:k})}[h(\boldsymbol{x}_{0:k})] = \int h(\boldsymbol{x}_{0:k})\ p(\boldsymbol{x}_{0:k} \mid \boldsymbol{y}_{0:k}) d\boldsymbol{x}_{0:k}, \tag{A.3}$$

for any function $h : \chi^{k+1} \to \mathbb{R}^{n_h}$ integrable with respect to $p(\boldsymbol{x}_{0:k} \mid \boldsymbol{y}_{0:k})$.
A recursive expression of the *posterior distribution* can be found recurring to the *prediction* and *update* steps. The former

$$p(\boldsymbol{x}_{0:k} \mid \boldsymbol{y}_{0:k-1}) = \int p(\boldsymbol{x}_k \mid \boldsymbol{x}_{k-1})\, p(\boldsymbol{x}_{0:k-1} \mid \boldsymbol{y}_{0:k-1})\, d\boldsymbol{x}_{k-1} \tag{A.4}$$

the latter according to the Bayes formula

$$p(\boldsymbol{x}_{0:k} \mid \boldsymbol{y}_{0:k}) = \frac{p(\boldsymbol{y}_k \mid \boldsymbol{x}_k) p(\boldsymbol{x}_{0:k} \mid \boldsymbol{y}_{0:k-1})}{p(\boldsymbol{y}_k \mid \boldsymbol{y}_{0:k-1})} \tag{A.5}$$

Where

$$p(\boldsymbol{y}_k \mid \boldsymbol{y}_{0:k-1}) = \int p(\boldsymbol{y}_k \mid \boldsymbol{x}_k) p(\boldsymbol{x}_{0:k} \mid \boldsymbol{y}_{0:k-1})\, d\boldsymbol{x}_k \tag{A.6}$$

However this results are more conceptual than practical, since only in few cases the integral, thus the quantities of interest, admit solution in closed-form. Nevertheless the recursive expression lay the foundation for the Sequential Monte Carlo method.

A.2 Monte Carlo Perfect Sampling

Given a set of samples $\{\boldsymbol{x}_{0:k}^1, \dots, \boldsymbol{x}_{0:k}^{N_s}\}$, also named *particle*, i.i.d. from the pdf of interest $p(\boldsymbol{x}_{0:k} \mid \boldsymbol{y}_{0:k})$ an empirical unbias estimation of the distribution and of the expectation (A.3) is given by:

$$\hat{p}(\boldsymbol{x}_{0:k}|\boldsymbol{y}_{0:k}) = \frac{1}{N_s}\sum_{1}^{N_s}\delta(\boldsymbol{x}_{0:k} - \boldsymbol{x}_{0:k}^i) \tag{A.7}$$

$$\hat{I}_{N_S}(h) = \frac{1}{N_s}\sum_{1}^{N_s} h(\boldsymbol{x}_{0:k}^i) \tag{A.8}$$

Thanks to the strong Law of Large Number (LLN) if the second moment is finite $\sigma_h^2 = E_{p(\boldsymbol{x}_{0:k} \mid \boldsymbol{y}_{0:k})}[h^2(\boldsymbol{x}_{0:k})] - I^2(h) < +\infty$, then $Var\left[\hat{I}_{N_S}(h)\right] = \frac{\sigma_h^2}{N_S}$, thus both the approximations converge to the respective real value almost surely:

$$\hat{p}(\boldsymbol{x}_{0:k}|\boldsymbol{y}_{0:k}) \xrightarrow[N_s\to\infty]{} p(\boldsymbol{x}_{0:k}|\boldsymbol{y}_{0:k})$$

$$\hat{I}_{N_S}(h) \xrightarrow[N_s\to\infty]{} I(h)$$

moreover, the central limit theorem is valid. Unfortunately it is usually almost impossible to sample efficiently from the desired distribution cause it is typically multivariate, non-standard and known up to a proportionality constant. A common approach is using Markov Chain Monte Carlo (MCMC) methods, however due to their iterative structure, they are not suitable for a recursive estimation problem. To avoid this problem importance sampling is a wide spread technique that allows to sample from a chosen distribution $\pi(\boldsymbol{x}_{0:k}^i|\, \boldsymbol{y}_{0:k})$ provided that weights $w_k^i\ i = 1, \dots, N_S$ are added to the particles:

$$\hat{p}(\boldsymbol{x}_{0:k}|\boldsymbol{y}_{0:k}) = \frac{1}{N_s}\sum_{i=1}^{N_s} w_k^i \delta(\boldsymbol{x}_{0:k} - \boldsymbol{x}_{0:k}^i) \tag{A.9}$$

$$w_k^i = \frac{p(\boldsymbol{x}_{0:k}^i|\,\boldsymbol{y}_{0:k})}{\pi(\boldsymbol{x}_{0:k}^i|\,\boldsymbol{y}_{0:k})} \tag{A.10}$$

Or alternatively by normalizing the weights:

$$\widetilde{w}_k^i = \frac{w_k^i}{\sum_{j=1}^{N_s} w_k^j} \tag{A.11}$$

$$\hat{p}(\boldsymbol{x}_{0:k}|\boldsymbol{y}_{0:k}) = \sum_{i=1}^{N_s} \widetilde{w}_k^i \delta(\boldsymbol{x}_{0:k} - \boldsymbol{x}_{0:k}^i) \tag{A.12}$$

However even in this case a recursive approach is not feasible since every time a new measurement arrives, all the trajectories of the weights of the particles must be reevaluated, hence the computational cost increases proportionally to time.

A.3 Particle Filtering

To overcome the problem a sequential approach is pursue, i.e., only the last step is updated when a new observation becomes available. Importance function $\pi(\boldsymbol{x}_{0:k}|\,\boldsymbol{y}_{0:k})$ is chosen such as:

$$\begin{aligned}\pi(\boldsymbol{x}_{0:k}|\,\boldsymbol{y}_{0:k}) &= \pi(\boldsymbol{x}_k|\,\boldsymbol{x}_{0:k-1},\,\boldsymbol{y}_{0:k})\pi(\boldsymbol{x}_{0:k-1}|\,\boldsymbol{y}_{0:k-1}) = \\ &= \pi(\boldsymbol{x}_0)\prod_{j=1}^{k}\pi(\boldsymbol{x}_j|\,\boldsymbol{x}_{0:j-1},\,\boldsymbol{y}_{0:j})\end{aligned} \tag{A.13}$$

Thus by decomposing the posterior as follow

$$\begin{aligned}p(\boldsymbol{x}_{0:k}|\boldsymbol{y}_{0:k}) &= \frac{p(\boldsymbol{y}_k|\,\boldsymbol{x}_{0:k},\boldsymbol{y}_{0:k-1})\,p(\boldsymbol{x}_{0:k}|\boldsymbol{y}_{0:k-1})}{p(\boldsymbol{y}_k|\boldsymbol{y}_{0:k-1})} \\ &= \frac{p(\boldsymbol{y}_k|\,\boldsymbol{x}_k)p(\boldsymbol{x}_k|\boldsymbol{x}_{k-1})}{p(\boldsymbol{y}_k|\boldsymbol{y}_{0:k-1})}p(\boldsymbol{x}_{0:k-1}|\boldsymbol{y}_{0:k-1})\end{aligned} \tag{A.14}$$

A recursive formulation for the weights (A.10) is given by:

$$w_k^i = w_{k-1}^i \frac{p(\boldsymbol{y}_k|\boldsymbol{x}_k^i)p(\boldsymbol{x}_k^i|\boldsymbol{x}_{k-1}^i)}{p(\boldsymbol{y}_k|\boldsymbol{y}_{0:k-1})\pi(\boldsymbol{x}_k^i|\boldsymbol{x}_{0:k-1}^i, \boldsymbol{y}_{0:k})} \tag{A.15}$$

Analogously a recursive formulation for the normalized weights (A.11)is given by:

$$\widetilde{w}_k^i = \widetilde{w}_{k-1}^i \frac{p(\boldsymbol{y}_k|\boldsymbol{x}_k^i)p(\boldsymbol{x}_k^i|\boldsymbol{x}_{k-1}^i)}{\pi(\boldsymbol{x}_k^i|\boldsymbol{x}_{0:k-1}^i, \boldsymbol{y}_{0:k})} \tag{A.16}$$

A typical choice for the importance function is the prior distribution $\pi(\boldsymbol{x}_{0:k}|\, \boldsymbol{y}_{0:k}) = p(\boldsymbol{x}_{0:k})$,i.e., $\pi(\boldsymbol{x}_k|\boldsymbol{x}_{0:k-1}, \boldsymbol{y}_{0:k}) = p(\boldsymbol{x}_k|\boldsymbol{x}_{k-1})$. Thus the effort of the updating step of the weights consist just in the evaluation of the likelihood based on (A.2):

$$\widetilde{w}_k^i = \widetilde{w}_{k-1}^i \, p(\boldsymbol{y}_k|\boldsymbol{x}_k^i) \tag{A.17}$$

Although the theoretic framework seems well posed, since a finite number of particle is used during real application problem still occur. *Degeneracy*, i.e., when the empirical distribution collapses on a single particle, usually happens. To avoid this problem, a *Resampling Step* is add to the algorithm to pass from an empirical distribution of weighted particles, to an empirical distribution of particles with equal weights. Section A.4 Sequential Importance Resampling (SIR) reports a scheme of the *Sequential Importance Resampling* (SIR) algorithm. During the last decades many improvements have been introduce to PF, such as Auxiliary Particle Filter (ASIR), Rao-Blackwellised Particle Filter (RBPF), Unscent Particle Filter (UPF) and Regularized Particle Filter (RPF) for specific kind of problem. For a better and complete description see (Arulampalam, et al., 2002) (Doucet, et al., 2008).

A.4 Sequential Importance Resampling (SIR)

1. Initialization $k = 0$
    - Sample $\boldsymbol{x}_0^i \sim p_0(\cdot)$ for $i = 1, \dots, N_s$ set $k = 1$
2. Importance sampling $k \geq 1$

For $i = 1, \dots, N_s$

- Sample $\breve{\boldsymbol{x}}_k^i \sim p(\cdot \mid \boldsymbol{x}_{k-1}^i)$
- Evaluate the weights $\tilde{w}_k^i = p(\boldsymbol{y}_k | \breve{\boldsymbol{x}}_k^i)$
- Normalized the importance weights

3. Systematic Resampling $k \geq 1$
   - Sample $U_1 \sim U\left[0, \frac{1}{N_s}\right]$
   - Define $U_i = U_1 + \frac{i-1}{N_s}$
   - Set $\boldsymbol{x}_k^i = \left\{\breve{\boldsymbol{x}}_k^j : \sum_{n=1}^{j-1} \tilde{w}_k^n \leq U_i < \sum_{n=1}^{j} \tilde{w}_k^n,\ j = 1, \dots, N_s\right\}$
   - Fixed $\tilde{w}_k^i = \frac{1}{N_s}$
   - $k \leftarrow k + 1$ and go to step 2.

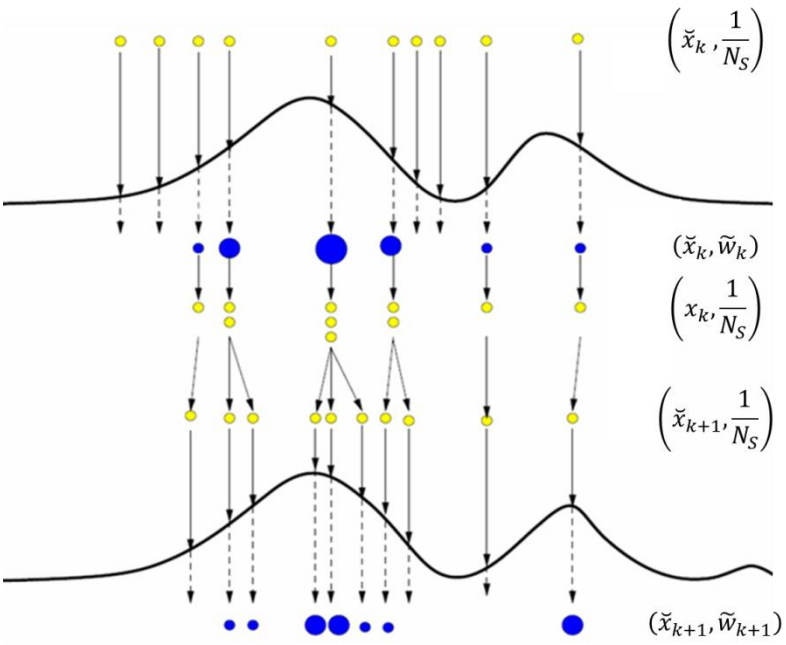

Fig. 0.1 Representation of a step of the SIR algorithm.